This is a preprint, the final version is subject to change, of the American Mineralogist (MSA)
Cite as Authors (Year) Title. American Mineralogist, in press.
(DOI will not work until issue is live.) DOI: http://dx.doi.org/10.2138/am-2016-5404

Crystal accumulation in a tilted arc batholith

Calvin G. Barnes[1]*, Nolwenn Coint[2], Aaron Yoshinobu[1]

[1]Department of Geosciences, Texas Tech University, Lubbock, TX 07409-1053, U.S.A.

[2]Geological Survey of Norway, PO Box 6315 Sluppen, 7491 Trondheim, Norway

*E-mail: cal.barnes@ttu.edu

Revision 1

ABSTRACT

The Wooley Creek batholith is a Late Jurassic, arc-related, calc-alkaline plutonic complex in the Klamath Mountain province of California. Post-emplacement tilting and erosion have exposed ~12 km of structural relief. The complex consists of an older (~159.1 Ma) lower zone (pyroxenite to tonalite) assembled by piecemeal emplacement of many magma batches, a younger (~158.2 Ma) upper zone (quartz diorite to granite), and a transitional central zone. In the lower zone, pyroxenes are too Fe-rich to be in equilibrium with a melt whose composition was that of the host rock. Mass balance calculations and simulations using rhyolite-MELTS indicate that these rocks are cumulates of pyroxenes and plagioclase ± olivine and accessory apatite and oxides. Percentages of interstitial melt varied from ~7.5–83%. The plagioclase/pyroxene ratios of cumulates vary considerably among the most mafic rocks, but are relatively uniform among quartz diorite to tonalite. This near-constant ratio results in compositional trends that mimic a liquid line of descent. In the upper zone, bulk-rock compositional trends are consistent with differentiation of andesitic parental magmas. Upward gradation from quartz dioritic to granitic

This is a preprint, the final version is subject to change, of the American Mineralogist (MSA)
Cite as Authors (Year) Title. American Mineralogist, in press.
(DOI will not work until issue is live.) DOI: http://dx.doi.org/10.2138/am-2016-5404

compositions, modeled via mass balance calculations and rhyolite-MELTS simulations, indicate that structurally lower parts of the upper zone are cumulates of hornblende and plagioclase ± biotite and accessory minerals, with 37–80% trapped melt. In contrast, the structurally higher part of the upper zone represents differentiated magma that escaped the subjacent cumulates, representing differentiated melt fractions remaining from 92–54%. The ratio of cumulate plagioclase/(plagioclase + mafic minerals) is ~0.48 among upper zone cumulates, mimicking a liquid line of descent.

The results suggest that compositional variation in many calc-alkaline plutons may be at least as representative of crystal accumulation as of fractional crystallization. If so, then the assumption that arc plutons geochemically resemble frozen liquids is dubious and should be tested on a case-by-case basis. Moreover, comparisons of plutonic rock compositions with those of potentially comagmatic volcanic rocks will commonly yield spurious results unless accumulation in the plutons is accounted for.

Keywords: calc-alkaline plutons, crystal accumulation, fractional crystallization, mass balance.

INTRODUCTION

The relationships between volcanic and plutonic rocks, and their original magmas, have been debated from early days of petrologic study (Daly, 1933; Wager et al., 1960; Gilluly, 1948) and are still a source of debate (e.g., Miller and Miller, 2002 Bachmann and Bergantz, 2004; Bachmann et al., 2007; Reubi and Blundy, 2009; Mills and Coleman, 2013; Lipman and Bachmann, 2015). Although bulk-rock compositional trends for volcanic rock suites are in many

This is a preprint, the final version is subject to change, of the American Mineralogist (MSA)
Cite as Authors (Year) Title. American Mineralogist, in press.
(DOI will not work until issue is live.) DOI: http://dx.doi.org/10.2138/am-2016-5404

cases comparable to those of plutonic suites (Coleman et al., 2012), it is clear from studies of layered mafic intrusions that bulk-rock compositions may reflect significant amounts of crystal accumulation (e.g., Wager and Brown, 1968; Naslund and McBirney, 1996). The importance of accumulation is even expressed in textural terminology used for mafic and ultramafic plutonic rocks (Wager et al., 1960; Hunter, 1996). In this paper, the term 'cumulate' is used to indicate a rock in which the abundance of one or more minerals is in excess of that which would occur during crystallization of a crystal-free parental melt. We use 'accumulation' to indicate the generic processes in which cumulate rocks form. Such processes include, but are not limited to, flow segregation (e.g., Komar, 1972; Paterson, 2009), gravitational settling or flotation (Darwin, 1844, Bowen, 1928), hindered settling and compaction (McKenzie, 1984, 1987; Lee et al., 2015), and filter pressing (Bowen, 1928).

Many calc-alkaline plutonic suites (that range from gabbro to granite) lack compositional layering and commonly have hypidiomorphic granular textures, a term that implies sequential growth of crystals, with no implications for crystal accumulation. Nevertheless, bulk-rock compositional features such as high concentrations of MgO, Al_2O_3, and Cr in calc-alkaline plutonic suites have been interpreted to indicate accumulation of ferromagnesian silicates, plagioclase, and augite or chromite, respectively (e.g., Beard, 1986; Barnes et al., 1995; Keller et al., 2015). A more significant question involves granitic (s.l.; we use the term granitic to refer to quartz-bearing intermediate to felsic rocks) suites whose bulk-rock compositions lie within well-defined compositional arrays. Traditionally, such compositional arrays have been interpreted to result from one or more differentiation processes, either at the level of emplacement or deeper (Hildreth and Moorbath, 1988; Sawka et al., 1990; Srogi and Lutz, 1997; Hildreth, 2004; Annen et al., 2006; Bédard et al., 2009; duBray et al., 2011). If crystal–liquid separation occurred at the

This is a preprint, the final version is subject to change, of the American Mineralogist (MSA)
Cite as Authors (Year) Title. American Mineralogist, in press.
(DOI will not work until issue is live.) DOI: http://dx.doi.org/10.2138/am-2016-5404

level of emplacement, then some plutonic rocks should be partial cumulates (e.g., Lee & Morton, 2015). However, if accumulation occurred in cotectic proportions, identification of cumulates on the basis of major element variation diagrams may be difficult because cumulate rock compositions will lie on a back-projection of the liquid line of descent (Deering and Bachmann, 2010). Alternatively, some authors have suggested that bulk compositions of upper crustal granitic rocks are commonly those of the magmas at the time of emplacement, with minor, local, post-emplacement differentiation (e.g., Coleman et al., 2012) or no differentiation at all (Mills, et al., 2012). The debate concerning relationships between volcanic and plutonic rocks, and in particular the importance of accumulation in plutons, is nicely summarized in two recent papers, both of which utilize global geochemical data sets. One group of authors (Glazner et al., 2015) concluded that plutonic rocks are "texturally modified samples of the same magmas that erupt", whereas the other group (Keller et al., 2015) concluded "…that fractional crystallization, rather than crustal melting, is predominantly responsible for the production of intermediate and felsic magmas, emphasizing the role of mafic cumulates as a residue of crustal differentiation". In addition, Keller et al. (2015) concluded accumulation of crystals from dacitic magmas is likely to yield mafic assemblages.

The distinction between these two concepts of pluton growth and development is significant for a number of reasons. For example, if granitic rocks are 'magmas frozen on emplacement', then compositional variation within a pluton or batholith must be related to magmatic processes in the deep crust and/or upper mantle (Annen et al., 2006; Clemens et al., 2010; Coleman et al., 2012) or to differentiation during transport. In these cases, a relationship between granitic plutons and volcanic rocks, the latter of which commonly show strong evidence for mixing, assimilation, and fractionation in middle- to upper-crustal reservoirs (e.g., Grunder et

al., 2006; Reubi & Blundy, 2009; Ruprecht et al., 2012; Singer et al., 2014, and many more), is probably tenuous. On the other hand, if some of the compositional variation within granitic suites is caused by in-situ crystal-liquid separation (e.g., Lee et al., 2015), it should be axiomatic that the plutons in question preserve evidence for differentiation processes that can be related to the compositions of volcanic rocks. Moreover, it should be possible on the basis of textural and/or compositional data to identify granitic rocks that are at least partial cumulates.

The paucity of widespread compositional layering in most granitic suites means that even if accumulation occurred during solidification of the magma, its physical effects (outcrop features and textures) may not be evident. Examples of cumulates in granitic plutons include one cited by Flood and Shaw (1979), who described K-rich cumulates at the base of a tilted granodiorite. More recently, a number of studies have identified granitic cumulate zones in stratified intrusions (e.g., Wiebe and Collins, 1998; Miller and Miller, 2002; Harper et al., 2004; Lux et al., 2007; Beane and Wiebe, 2012) and schlieren and related structures are commonly thought to be cumulate in origin (Vernon and Paterson, 2008). These observations lead to the question: are cumulates in granitic plutons restricted to special cases such as those cited here, or are they significantly more common? The answer to this question is important, because petrogenetic interpretations of plutonic rock suites depend on how petrologists interpret rock compositions: do they represent melts, combinations of melt plus accumulated crystals, or pure cumulates? Moreover, considering the conflicting conclusions reached on the basis of studying compositional trends based on global data sets, it may be more instructive to investigate the importance of crystal accumulation in individual plutonic suites (e.g., Lee and Morton, 2015).

Deering & Bachmann (2010) discussed problems involved in distinguishing cumulate granitic rocks from ones that represent crystallized melt. They used trace element trends to

This is a preprint, the final version is subject to change, of the American Mineralogist (MSA)
Cite as Authors (Year) Title. American Mineralogist, in press.
(DOI will not work until issue is live.) DOI: http://dx.doi.org/10.2138/am-2016-5404

identify probable liquid lines of descent caused by fractional crystallization, and placed particular emphasis on changes in slope which signify addition of a new phase in the fractionating assemblage (Bowen, 1928). They pointed out that the use of trace element trends is appropriate because in many intermediate to felsic systems, multiple saturation of feldspars + mafic silicates ± quartz results in melt compositions that follow a nearly linear cotectic path, leading to linear compositional arrays in binary diagrams. These relationships were expanded upon by Gelman et al. (2014), who developed algorithms for numerical modeling of trace element variation in melts and accumulated crystals. Moreover, in a regional study of the Peninsular Ranges batholith, Lee and Morton (2015) concluded that many granitic rocks may superficially resemble frozen liquids, even though many of the rocks in fact contain large percentages of cumulate minerals.

The approach used by Deering and Bachmann (2010) is conceptually straightforward; however, situations may exist in which a change of slope in plots of bulk-rock compositions does not exist, either for major or trace elements. In such cases, other means of assessing the existence and proportions of cumulate minerals must be found (e.g., Srogi and Lutz, 1996, 1997).

This contribution is a study of crystal accumulation in tilted plutonic system, the Wooley Creek batholith (WCb) in which approximately 12 km of structural relief is exposed. The WCb is an excellent place to assess accumulation because it encompasses a wide range of bulk compositions (pyroxenite to granite) and is crudely zoned from lowermost gabbro, diorite, and tonalite to uppermost granite, with dikes in the structurally high 'roof zone' representing leaks from the underlying magmas. Our results indicate that the great majority of rocks in the batholith are partial cumulates. These results call for caution when interpreting bulk-rock compositional trends of plutonic suites as representative of differentiation trends.

This is a preprint, the final version is subject to change, of the American Mineralogist (MSA)
Cite as Authors (Year) Title. American Mineralogist, in press.
(DOI will not work until issue is live.) DOI: http://dx.doi.org/10.2138/am-2016-5404

GEOLOGIC SETTING

The Wooley Creek batholith (Fig. 1) is a Late Jurassic plutonic complex in the Klamath Mountain province of northern California. The province is an accretionary orogen (Irwin, 1960, 1972; Snoke and Barnes, 2006) in which tectonostratigraphic terranes were amalgamated from at least Cambrian through Late Jurassic time. The terranes are interpreted to be separated by regional faults/shear zones, generally with low-angle reverse displacement.

The WCb intruded three terranes of the western Paleozoic and Triassic belt (Irwin, 1972); from structurally lowest to highest, they are Rattlesnake Creek terrane, western Hayfork terrane, and eastern Hayfork terrane. Descriptions of these host terranes may be found in Irwin (1972), Wright (1982), Wright and Fahan (1988), Wright and Wyld (1994), and Donato et al. (1996). During the Nevadan orogeny, the WCb and its host terranes were thrust over rocks of the western Jurassic belt (Jachens et al., 1986; Snoke and Barnes, 2006). Regional doming centered to the northeast of the batholith (Barnes, 1983; Mortimer and Coleman, 1985; Barnes et al., 1986b, their Fig. 1) resulted in tilting of the overlying terranes (and plutons). In the case of the WCb, tilting and subsequent erosion exposed ~12 km of structural relief in the pluton, with the deepest levels (paleodepth ~22 km) in the northeast and the shallowest (paleodepth ~10 km) in the south and southwest (Fig.1; Barnes et al., 1986b).

Wooley Creek batholith

The batholith can be divided into lower and upper zones, which are locally separated by a transitional ‘central zone’ (Fig. 1; Coint et al., 2013b). Chemical abrasion-ID-TIMS U-Pb dating on zircon (Coint et al., 2013b) indicated that the lower and upper zones are temporally distinct,

This is a preprint, the final version is subject to change, of the American Mineralogist (MSA)
Cite as Authors (Year) Title. American Mineralogist, in press.
(DOI will not work until issue is live.) DOI: http://dx.doi.org/10.2138/am-2016-5404

with lower zone ages of 158.99 ± 0.17 to 159.28 ± 0.17 Ma and upper zone ages of 158.21 ± 0.17 to 158.25 ± 0.46 Ma (all uncertainties are 2σ). Two samples from the central zone gave CA-ID-TIMS ages of 158.95 ± 0.34 and 158.30 ± 0.16 Ma; the former age is identical to those of the lower zone and the latter to those of the upper zone. Thus, the central zone was formed by magmas from both adjacent zones of the batholith. Discontinuous selvages of diorite and quartz diorite crop out along the western and southern contacts of the batholith (Fig. 1). These selvages are texturally and mineralogically similar to rocks of the lower zone and are considered to be remnants of lower-zone type magmas into which the upper zone magmas were emplaced (Coint et al., 2013a, b).

The western and southwestern contact of the batholith is termed the 'roof zone' (Barnes et al., 1986). This contact zone is quite variable: in some locations granodiorite or granite of the upper zone is in direct, sharp contact with the host rocks, whereas in other locations the mafic selvages cited above, some with abundant xenoliths, separate the host rocks from typical upper zone rocks. Numerous fine- to medium-grained basaltic, andesitic, dacitic and rhyodacitic dikes are present in the roof zone. Although mafic roof-zone dikes were not observed to cut the pluton, two-pyroxene andesitic dikes both cut and are cut by upper-zone granodiorite. A second set of andesitic dikes, with phenocrysts of hornblende, augite, and plagioclase, intrude the roof-zone host rocks, but were not seen to cut the pluton. Similarly, medium-grained dacitic to rhyodacitic roof-zone dikes do not cut the pluton. These dikes carry phenocrysts of plagioclase and hornblende ± biotite ± quartz. On the basis of similar bulk-rock and phenocryst compositions, the dacitic and rhyodacitic dikes were interpreted to represent magma leaked from an upper-zone reservoir (Barnes et al., 1990; Coint et al., 2013a, b).

This is a preprint, the final version is subject to change, of the American Mineralogist (MSA)
Cite as Authors (Year) Title. American Mineralogist, in press.
(DOI will not work until issue is live.) DOI: http://dx.doi.org/10.2138/am-2016-5404

The lower zone is heterogeneous at the outcrop scale, consisting of gabbroic to tonalitic rocks, with blocks and dike-like masses of pyroxenite and melagabbro, sparse mafic magmatic enclaves (mme), and fine- to medium-grained synplutonic dikes. Unaltered lower zone gabbroic to tonalitic rocks typically contain augite and orthopyroxene with late biotite ± hornblende and accessory K-feldspar, Fe-Ti oxides, apatite, and zircon. A few of the mafic samples contain relict olivine (Barnes, 1983; 1987; Coint et al., 2013b). Pyroxenites and melagabbros consist of augite and orthopyroxene ± plagioclase ± olivine (~Fo70) ± hornblende ± quartz ± Fe-Ti oxides. In general, plagioclase shows oscillatory-normal zoning, with cores as calcic as An_{79} and rims as sodic as An_{32} (Fig. 2A; Barnes, 1987). The range of zoning varies from fewer than 10 mole % An to nearly 50 mole % An (Fig. 2A). Lower zone rocks are characterized by moderate to strong magmatic foliation formed by aligned plagioclase and pyroxenes (Barnes, 1983; Coint et al., 2013b). Deformation locally continued to near-solidus conditions, as indicated by bent plagioclase and strained quartz.

Field relationships, bulk-rock compositions, and detailed study of augite compositions indicate that the heterogeneity of the lower zone is due to emplacement of multiple magma batches, with or without magma mixing (Coint et al., 2013a, b). It is clear that lower-zone rocks were not derived from a single parental composition. Instead, they crystallized from many small- to moderate-volume magma batches.

The upper zone grades from biotite hornblende quartz diorite in its structurally lowest part (ca. 14 km paleodepth) to biotite hornblende granite in its uppermost parts (ca. 10 km paleodepth; Fig. 1). All samples are characterized by hypidiomorphic granular texture and contain phenocrysts of plagioclase and hornblende ± biotite. The upward compositional variation is expressed as a decrease in abundance of the mafic minerals, increase in abundances of quartz

This is a preprint, the final version is subject to change, of the American Mineralogist (MSA)
Cite as Authors (Year) Title. American Mineralogist, in press.
(DOI will not work until issue is live.) DOI: http://dx.doi.org/10.2138/am-2016-5404

and K-feldspar, and a change in K-feldspar habit from interstitial to poikilitic (Barnes, 1983; Coint et al., 2013b). Relict augite is sparsely present as cores in hornblende. Foliation in upper zone rocks, which is formed by aligned plagioclase and hornblende, varies from moderate to absent. The intensity of the foliation increases structurally downward.

The central zone is characterized by a series of intrusive sheets from 1–10 m width that range from gabbro to tonalite (Coint et al., 2013a). Mineral and bulk-rock compositions along with textural features indicate that the majority of central zone samples are petrologically linked to the upper zone (Coint, 2013a, b). Most samples contain biotite and hornblende as ferromagnesian phases, but relict augite and opx are common (Barnes, 1983). The central zone was also the site of emplacement of locally abundant synplutonic mafic dikes. These dikes are mainly basaltic, are fine- to medium-grained, and are commonly deformed and disrupted in both ductile and brittle fashion, leading to formation of linear swarms of mme (Barnes et al., 1986b).

GEOCHEMISTRY

The geochemical data and descriptions of compositional variation in the WCb have been presented in detail elsewhere (Barnes, 1983; Barnes et al., 1990; Coint et al., 2013b). In this paper, bulk-rock and mineral compositions are used to subdivide lower and upper zone rocks and to identify potential cumulate compositions.

Lower zone. It is possible to identify two groups of lower zone rocks, one of which can be further subdivided. The most mafic group consists of pyroxenite, melagabbro, gabbro, and diorite (including quartz-bearing diorite). In Figure 3, this group is subdivided into a pyroxenite–melagabbro subgroup and a gabbro–diorite subgroup. Taken together, the pyroxenite–diorite group rocks have SiO_2 contents less than 54 wt% and most have MgO contents > 7 wt% (Fig.

This is a preprint, the final version is subject to change, of the American Mineralogist (MSA)
Cite as Authors (Year) Title. American Mineralogist, in press.
(DOI will not work until issue is live.) DOI: http://dx.doi.org/10.2138/am-2016-5404

3A). The one exception is a leucocratic, synplutonic, plagioclase-rich biotite diorite dike with 2.1 wt% MgO and 23.6% Al_2O_3. Texturally, this sample (58) is a plagioclase cumulate.

The other lower-zone subgroup encompasses quartz diorite and tonalite, with silica contents from ~53–60 wt%. Compositions of this subgroup show negative correlation between SiO_2 and MgO, TiO_2, and Sr (Fig. 3) and no correlation between SiO_2 and Na_2O (Fig. 3B) or total alkalis, ($Mg/Mg+Fe_{total}$), and Hf (not shown). Average plagioclase composition is <55% An in quartz diorite and tonalite, although there is broad overlap in plagioclase compositions in this group compared to the pyroxenite–diorite group (Fig. 2A). A few samples were analyzed for trace element concentrations in plagioclase (Table 1), in which Sr contents vary from ~470 to ~700 ppm (Fig. 3D).

Pyroxene compositions Fig. 2B) show progressive enrichment in Fe from pyroxenitic to tonalitic rocks, as would be expected in a suite of differentiating magmas. However, comparison of Mg/Fe values of orthopyroxene (opx) with the Mg/Fe values of the rocks in which the pyroxenes occur shows that the opx cannot have been in equilibrium with a melt whose composition was that of the bulk rock (Fig. 3E). Similarly, Figure 3F compares measured CaTs, EnFs, and DiHd components in augite with the values predicted assuming the augite was in equilibrium with a melt of the bulk-rock composition (after Putirka, 2008). From these diagrams, it is clear that neither opx nor augite in lower-zone rocks were in equilibrium with melts whose compositions were the same as the bulk-rock compositions, because the latter are too rich in Mg.

Detailed trace element analysis of lower-zone augite (Coint et al., 2013a) showed that: (1) some samples show well-defined trace element variation, (2) other samples contain two or more populations of augite, and most significantly, (3) the rare earth elements (REE) of augite from lower zone samples vary in abundance, shape of the REE pattern, and dimensions of the Eu

This is a preprint, the final version is subject to change, of the American Mineralogist (MSA)
Cite as Authors (Year) Title. American Mineralogist, in press.
(DOI will not work until issue is live.) DOI: http://dx.doi.org/10.2138/am-2016-5404

anomaly (Fig. 2C), with more than a 10-fold variation in augite REE within a single sample. These features led Coint et al. (2013a) to conclude that lower zone magmas could not be related to a single parental composition, and certainly not to a single parental magma.

Central zone. The central zone is the most heterogeneous part of the WCb, primarily because of numerous synplutonic dikes and swarms of mafic magmatic enclaves (e.g., Barnes et al., 1986a; Coint et al., 2013b). The majority of synplutonic dikes have SiO_2 less than 56 wt% (Fig. 3A) and tend to show wide scatter in major element compositions, whereas the central zone host rocks to these dikes have bulk-rock SiO_2 contents from 51.2 to 65.6 wt% (Fig. 3) and coherent major element trends (Coint et al., 2013b). Average plagioclase compositions range from An_{50} to An_{46}, with some cores as calcic as An_{60} and rims as sodic as An_{17} (Fig. 2A).

Upper zone. Samples of the upper zone range from quartz diorite to granite. Their bulk SiO_2 contents vary from 53.1 to 70.1 wt % (Fig. 4; Coint et al., 2013b, their Fig. 8). The An contents in plagioclase decrease as a function of bulk SiO_2 contents (Barnes, 1987), with average An contents varying from An_{50} to An_{30}, cores as calcic as An_{57} and rims as sodic as An_{19} (Fig. 2A). Trace element data on plagioclase from two samples (Table 1) indicate Sr contents from ~750 to ~1160 ppm. In contrast to the highly variable REE compositions of augite in the lower zone, hornblende in upper zone rocks shows very similar REE patterns and abundances, although in general the size of the negative Eu anomaly increases from core to rim (Coint et al., 2013a, their Fig. 2D).

The variation of several elements, including Al_2O_3 (Fig. 4A) is notable because in the samples of the upper zone with $SiO_2 < 60$ wt%, Al_2O_3 contents are uncorrelated with SiO_2 or other differentiation indices. In contrast, upper zone samples with > 60 wt% SiO_2 show a decrease in Al_2O_3 as SiO_2 increases. The plot of Hf versus SiO_2 (Fig. 4B) shows a somewhat

This is a preprint, the final version is subject to change, of the American Mineralogist (MSA)
Cite as Authors (Year) Title. American Mineralogist, in press.
(DOI will not work until issue is live.) DOI: http://dx.doi.org/10.2138/am-2016-5404

similar relationship. With the exception of three upper zone samples, Hf increases with SiO_2 in rocks with <60 wt% but decreases as SiO_2 increases from 60 to 74 wt%. This change from increasing to decreasing Hf contents is characteristic of the onset of zircon fractionation.

Roof zone dikes. Mineral and bulk-rock compositions of the roof zone dikes are discussed in detail elsewhere (Barnes, 1987; Barnes et al., 1990; Coint et al., 2013a). Compared to mafic synplutonic dikes, mafic roof-zone dikes generally have similar MgO, higher SiO_2, and lower TiO_2 (not shown). The dacitic and rhyodacitic dikes are generally similar in composition to upper-zone rocks and share similar plagioclase (Fig. 2E) and hornblende compositions (Coint et al., 2013a, their Fig. 8).

CRYSTAL ACCUMULATION IN THE WOOLEY CREEK BATHOLITH

Within the upper zone, the uniformity of texture and mineral compositions, combined with upward change in rock type from quartz diorite to granite, suggest evolution from a single magma reservoir (Coint et al., 2013a, b). If this was the case, then the most mafic rocks in this zone should have chemical characteristics of cumulates and the most evolved rocks should represent differentiates, assuming that not all such differentiated magmas rose to higher crustal levels. These conclusions should be supported by changes in the slope of trends in variation diagrams.

In contrast, because the lower zone was constructed from multiple magma batches with a range of compositions, it is difficult to interpret compositional trends among lower-zone rocks as being related to in-situ magma differentiation. The compositional variation seen in lower-zone rocks led previous workers (Barnes et al., 1990; Coint et al., 2013b) to suggest that many lower-zone samples are cumulates. In the following sections, possible explanations for compositional

This is a preprint, the final version is subject to change, of the American Mineralogist (MSA)
Cite as Authors (Year) Title. American Mineralogist, in press.
(DOI will not work until issue is live.) DOI: http://dx.doi.org/10.2138/am-2016-5404

299 variation in the lower and upper zone magmas are modeled via mass balance calculations and
300 tested using rhyolite-MELTS and trace element mass balance calculations.
301 Lower zone: pyroxenite–diorite group. The high MgO and low Al_2O_3 of these rocks, combined
302 with the lack of correlation with SiO_2 or other indices of differentiation (Fig. 3) suggest that the
303 bulk compositions do not represent a differentiation trend. Instead, many of these sample
304 compositions plot within or to the low-SiO_2 side of the field bounded by compositions of augite,
305 opx, and plagioclase (Fig. 3). In addition, there is scant overlap of the pyroxenite–diorite
306 compositions with potential basaltic melts, as represented by the fine-grained synplutonic dikes
307 (e.g., Fig. 3A). These geochemical features can be explained if the coarse-grained pyroxenite–
308 diorite group rocks are cumulate in origin, and this explanation is consistent with the lack of
309 equilibrium relationships between opx–bulk-rock and augite–bulk-rock compositions (Fig. 3E, F,
310 respectively). This discrepancy results from the fact that the pyroxenes are too Fe-rich relative to
311 the bulk-rock composition. Explanations for this compositional mismatch include: (1) the bulk-
312 rock compositions result from mixing of an evolved, pyroxene-phyric magma with an aphyric
313 Mg-rich magma. The effects of mixing are locally evident. For example, Cr contents in some
314 augite crystals show zoning reversals interpreted to result from magma mixing (Coint et al.,
315 2013a). Likewise, crossing tie lines between coexisting pyroxene compositions (Fig. 2A) suggest
316 local mingling. Nevertheless, batch-wise emplacement of lower zone magmas and the paucity of
317 prominent zoning reversals in plagioclase (Barnes, 1987) suggest that mixing within lower zone
318 magmas was minor. (2) The pyroxenes equilibrated with Fe-rich residual melts. Percolation of
319 Fe-rich melts through lower-zone magmatic mushes would be expected to result in samples rich
320 in Fe-Ti oxides. However, oxide-rich samples have not been found. (3) The majority of

This is a preprint, the final version is subject to change, of the American Mineralogist (MSA)
Cite as Authors (Year) Title. American Mineralogist, in press.
(DOI will not work until issue is live.) DOI: http://dx.doi.org/10.2138/am-2016-5404

pyroxenite–diorite samples are cumulates, in which the accumulating phases were augite and orthopyroxene ± plagioclase ± olivine ± accessory minerals.

If rocks of the lower-zone pyroxenite–diorite group are cumulates, then their bulk compositions must be the sum of cumulus minerals augite ± opx ± plagioclase ± olivine ± Fe-Ti oxides, plus a melt phase that was in equilibrium with the cumulus minerals. For this study, we compared Mg/Fe in augite with Mg/Fe of fine-grained rocks in the WCb system (mafic roof-zone dikes, synplutonic dikes, and sheets in the central zone). Four rocks had Mg/Fe values consistent with equilibrium with lower-zone pyroxenes: MMB-236A, MMB-555, MMB-771, and WCB-4809. Compositions of these samples are plotted as blue stars in Figure 3, which shows that their compositions lie within or near the 'cumulate box' formed by the compositions of pyroxenes and plagioclase.

Lower zone quartz diorite–tonalite group. As with the pyroxenite–diorite group, pyroxenes in the lower zone quartz diorite–tonalite group cannot have been in equilibrium with melts having the compositions of the bulk rocks (Fig. 3E, F). It is thus logical to assume that these rocks are cumulate. However, because nearly all quartz diorite–tonalite compositions lie on the high-silica side of the cumulate box, it is also logical that the cumulate minerals in these rocks were in equilibrium with a melt more siliceous than the most SiO_2-rich tonalite. Two fine-grained rocks. roof-zone dike MMB-548 and central zone sheet MMB-777A (shown was green stars in Fig. 3), have Mg/Fe appropriate for equilibrium with pyroxenes in lower zone tonalites; both samples have dacitic bulk compositions (Table 2).

Lower zone mass balance models. If bulk compositions of lower zone samples are, in part, due to crystal accumulation, and if the samples identified above represent potential interstitial melts, then it should be possible to mass balance rock compositions with the compositions of the

This is a preprint, the final version is subject to change, of the American Mineralogist (MSA)
Cite as Authors (Year) Title. American Mineralogist, in press.
(DOI will not work until issue is live.) DOI: http://dx.doi.org/10.2138/am-2016-5404

cumulate phases and an interstitial melt phase. Results of major element mass balance calculations (least-squares model of Bryan et al., 1969) indicate that such accumulation is possible (Table 3). For the pyroxenite–diorite group, proportions of interstitial melt (represented by blue stars in Fig. 3) range from ~7% to 83%. In most calculations, the cumulate phases are augite, opx, and plagioclase ± olivine ± Fe-Ti oxides. The proportions of cumulate plagioclase (compared to total cumulates) vary from 2–54% and average 30 ± 23%. It is noteworthy that use of MMB-771 composition as the interstitial melt requires accumulation of An_{85} plagioclase (Table 3). However, plagioclase this calcic is uncommon in lower zone samples (Fig. 2E), suggesting that MMB-771 is not an appropriate proxy for interstitial melt.

Mass balance calculations for the quartz diorite–tonalite group indicate that augite, opx, and plagioclase are cumulate phases, and that small proportions of Fe-Ti oxides were also cumulate (Table 3). Although the choice of interstitial melt composition (green stars in Fig. 3) clearly affects the calculated percentage of melt, the calculations are consistent with ~30–70% of quartz diorite–tonalite samples being cumulate minerals. Moreover, the proportions of cumulate plagioclase (compared to total cumulates) vary over a narrow range of 41–57% and average 52 ± 5%.

The mass balance calculations indicate that the ratio of cumulate [plagioclase/(plagioclase + pyroxene)] in rocks of the pyroxenite–diorite group varies widely, whereas the same ratio in rocks of the quartz diorite–tonalite group has a relatively limited range of values (Fig. 5; Table 3). These differences are consistent with the wide compositional scatter observed in the pyroxenite–diorite group (Fig. 3), and suggest the potential for a range of magmatic conditions and/or accumulation processes that permitted preferential segregation of pyroxene versus plagioclase. In contrast, the comparatively small range of the ratio of cumulate

This is a preprint, the final version is subject to change, of the American Mineralogist (MSA)
Cite as Authors (Year) Title. American Mineralogist, in press.
(DOI will not work until issue is live.) DOI: http://dx.doi.org/10.2138/am-2016-5404

minerals in the quartz diorite–tonalite group (Fig. 5) suggests that separation of cumulate minerals from their host magmas was in approximately cotectic proportions.

Tests of lower zone mass balance calculations: *pyroxenite–diorite group*. The major-element mass balance models show that use of compositions of samples MMB-555 and WCB-4809 as proxies for interstitial melts provide adequate fits (low r^2 values) and match plagioclase compositions, whereas use of sample MMB-771 requires plagioclase more calcic than is typical of the natural samples. To further test the viability of the first two compositions as interstitial melt proxies, simulations of magma crystallization were made using rhyolite-MELTS (Gualda and Ghiroso, 2014, 2015) in an attempt to match the anorthite contents of plagioclase and Mg/Fe values of opx and augite (supplementary Appendix). The models were run at 500 MPa and NNO oxygen buffer; values consistent with conditions in the lower zone (Barnes, 1987). The H_2O contents used in the models varied from 1–5 wt%. For proxy melt compositions MMB-555 and WCB-4809, matches to plagioclase An contents and pyroxene Mg/Fe values were achieved at 3–4 wt% H_2O. These models indicate liquidus temperatures from 1165–1136°C, augite as the liquidus phase, and plagioclase crystallization at least 140–150°C below the liquidus. At the plagioclase liquidus the proportion of melt was ≥ 60 volume% and the melt density was ~1000 kg/m^3 lower than that of the bulk solid. This density difference suggests that migration of the melt away from the solid was possible, and could leave a pyroxenitic to gabbroic cumulate.

Tests of lower zone mass balance calculations: *quartz diorite–tonalite group*. The proxy compositions for interstitial melt (MMB-548 and MMB-777A) were modeled using rhyolite-MELTS at 400 MPa, NNO, and H_2O contents of 1–5 wt% (supplementary Appendix). Liquidus temperatures decreased with increasing H_2O contents from 1168–1084°C for composition MMB-548 and from 1129–1041°C for composition MMB-777A. Orthopyroxene was the

This is a preprint, the final version is subject to change, of the American Mineralogist (MSA)
Cite as Authors (Year) Title. American Mineralogist, in press.
(DOI will not work until issue is live.) DOI: http://dx.doi.org/10.2138/am-2016-5404

liquidus phase in all simulations and compositional matches of Mg/Fe in opx and augite were achieved in the 900–950°C range at 3–5 wt% H_2O and 980–1040°C at 2% H_2O. In simulations run at 1% H_2O, opx Mg/Fe values were matched at 1000°C, but calculated augite compositions were too Fe rich at any temperature. Modeled plagioclase stability in systems with 2% H_2O is 60–80°C below the liquidus temperature and plagioclase compositions were in the An_{56}–An_{54} range for all models. Rim compositions of plagioclase in the quartz diorite–tonalite group are ~An_{45}, which corresponds to T of ~950°C in models at 2% H_2O. At this condition, melt constitutes ~70% of the volume and the difference between densities of the bulk solid and the melt is ~560 kg/m^3. The best matches to mineral compositions indicate that rocks of quartz diorite–tonalite group are partial cumulates from magmas with relatively low H_2O contents (~2 wt%). This conclusion is consistent with the fact that hornblende is absent in some quartz diorite–tonalite group samples; biotite is the late-stage hydrous phase (Barnes, 1987), indicating that H_2O contents were relatively low (<3–4%; e.g., Naney, 1983). Variable proportions of separation of melt from pyroxene and plagioclase could result in the range of bulk compositions seen in the quartz diorite–tonalite group.

A second set of tests involves mass-balance of the REE. These tests used the proportions of cumulate minerals determined from major element mass balance calculations to sum the REE abundances of augite, opx, plagioclase, and an interstitial melt in an attempt to match the bulk-rock composition (Fig. 6). For each mass balance, two compositions of interstitial melt were used. One composition was that of the rock used as a proxy for interstitial melt; the other was calculated on the basis of average augite REE compositions in the sample of interest. In general, interstitial melt compositions calculated on the basis of augite REE resulted in close fits to the

This is a preprint, the final version is subject to change, of the American Mineralogist (MSA)
Cite as Authors (Year) Title. American Mineralogist, in press.
(DOI will not work until issue is live.) DOI: http://dx.doi.org/10.2138/am-2016-5404

bulk-rock data (Fig. 6A, B, D). However, in samples with a wide range of augite REE contents large misfits can occur (e.g., MMB-30; Fig. 6C).

In summary, it is first worth reiterating geological and petrological observations, which indicate that assembly of the lower zone was a piecemeal process and undoubtedly involved a diversity of magmas ranging from basaltic andesite to dacite. Moreover, some magma batches mixed/mingled at the level of emplacement, others did not. Nevertheless, the major element mass balance calculations coupled with rhyolite-MELTS simulations suggest that many/most lower-zone samples are partial cumulates. Interstitial melts in the pyroxenite–diorite group were broadly basaltic andesite in composition, whereas interstitial melts in the quartz diorite–tonalite group were dacitic. The rhyolite-MELTS simulations suggest that the basaltic andesite melts were richer in H_2O than the dacitic ones. If so, this difference in H_2O content precludes a direct relationship between the pyroxene–diorite group and the quartz diorite–tonalite group.

Results of the rhyolite-MELTS simulations provide estimates of the crystal fraction at any specific temperature. For simulations involving quartz diorite–tonalite at 2 wt% H_2O, observed mineral compositions and approximate cumulate proportions are reproduced at ~1000°C, a temperature that is consistent with two-pyroxene geothermometry (Barnes, 1987). In this temperature range, the simulations indicate crystal mass fractions of ~17–22%. If the various assumptions embedded in the preceding discussion are appropriate, then rocks of the quartz diorite–tonalite group represent accumulation of as little as 10% to as much as 50% crystals.

ACCUMULATION AND FRACTIONAL CRYSTALLIZATION IN THE UPPER ZONE

The striking similarity of hornblende trace element compositions in the upper zone led Coint et al. (2013a) to suggest that the upper zone evolved from an essentially homogeneous magma. [N.b., Coint et al. (2013a) did not suggest that the upper zone formed from a single

This is a preprint, the final version is subject to change, of the American Mineralogist (MSA)
Cite as Authors (Year) Title. American Mineralogist, in press.
(DOI will not work until issue is live.) DOI: http://dx.doi.org/10.2138/am-2016-5404

magma batch, but instead from magmas of similar/identical compositions that coalesced and were mixed due to injection of basaltic magmas at the base of the zone (cf., Burgisser and Bergantz, 2011).] If the upper zone magma was initially homogeneous, then upward zoning from quartz diorite and tonalite to granite requires that some upper zone rocks are cumulates, others represent fractionated magmas, and a few may be representative of the original (parental) magma composition. Compositional variation of the major elements is characterized by nearly linear trends (Coint et al., 2013b), however, for several trace elements the compositional trends show changes from positive to negative slopes with increasing SiO_2 (Fig. 4; Coint et al., 2013b), which may be interpreted as constituting evidence for crystal-liquid separation (e.g., Bowen, 1928; Deering and Bachmann, 2010; Lee and Morton, 2015).

If the upper zone was related to a single magma *composition*, the parental magma must lie at SiO_2 contents lower than the value at which incompatible elements become compatible (the 'peak' in variation diagrams). For this discussion, the composition of roof zone andesitic dike sample MMB-612 was used because it lies near the change in slope in variation diagrams (Fig. 4), contains phenocrysts of augite, hornblende, and plagioclase, and shows evidence for late-stage biotite stability. Use of this composition required that mass balance models be of two types. Compositions of upper zone samples more mafic than MMB-612 were modeled in terms of accumulation, in which the presumed cumulate rock composition was calculated as the sum of crystals and 'melt' (= MMB-612). In these calculations, the proportion of crystals represents the cumulate fraction of the modeled rock composition. In contrast, compositions of samples more felsic than MMB-612 were modeled in terms of fractional crystallization, in which the 'parental' composition (MMB-612) was calculated as the sum of crystals plus evolved rock compositions.

This is a preprint, the final version is subject to change, of the American Mineralogist (MSA)
Cite as Authors (Year) Title. American Mineralogist, in press.
(DOI will not work until issue is live.) DOI: http://dx.doi.org/10.2138/am-2016-5404

In these calculations, the proportion of evolved rock used in the calculation represents the melt fraction at the end of fractionation.

Mass balance calculations of accumulation were of two types. One set of calculations considered only plagioclase and hornblende ± accessory minerals as cumulate phases. Successful calculations (lowest sum of squares of residuals) yielded proportions of interstitial melt from 0.49 to 0.88. A characteristic of these results was that the composition of the cumulate plagioclase was in the range An_{60}–An_{77}, much more calcic than is observed in the rocks (Fig. 2E). A second set of calculations (Table 4) considered augite, plagioclase, hornblende, and biotite as potential cumulate minerals, along with accessory phases. These calculations yielded proportions of interstitial melt from 0.37 to 0.86, slightly lower than results from the first set of models, and compositions of cumulate plagioclase in the range observed in the rocks: from $An_{43–50}$.

Mass balance calculations for fractional crystallization used hornblende + plagioclase ($An_{43–56}$) ± biotite and accessory minerals as fractionating phases (Table 4). The calculated fraction of melt remaining varied from ~92% to ~54%.

Testing upper zone mass balance calculations using rhyolite-MELTS is complicated by the fact that solution models for hornblende are not available and in some cases the program has difficulty modeling plagioclase compositions. Simulations were run using MMB-612 (300 MPa, NNO) over a range of H_2O contents from 2–5 wt%. The results suggest that at H_2O contents greater than 3 wt%, plagioclase crystallization occurs at unrealistically low temperatures (<950°C), which results in excessive Al_2O_3 enrichment in the melt (≥ 18wt%). In contrast, the rhyolite-MELTS simulation with 2 wt% H_2O indicates plagioclase stability at 1040°C at a silica content of the melt of ~61.9 wt%. These results, and the major element mass balance

This is a preprint, the final version is subject to change, of the American Mineralogist (MSA)
Cite as Authors (Year) Title. American Mineralogist, in press.
(DOI will not work until issue is live.) DOI: http://dx.doi.org/10.2138/am-2016-5404

480 calculations, are consistent with bulk-rock compositions. For example, upper zone samples with
481 SiO_2 < 62 wt% show a wide scatter of Al_2O_3 contents (Fig. 4A), which would be expected if the
482 low-SiO_2 samples contained variable proportions of cumulate plagioclase and hornblende,
483 whereas Al_2O_3 decreases in samples with higher SiO_2. Similarly, Hf increases in samples with
484 SiO_2 < 60 wt% but decreases in samples with higher SiO_2 contents, consistent with zircon ±
485 hornblende fractionation (also see Coint et al., 2013a, b). Barium abundances also decrease
486 above SiO_2 contents of ~65 wt%, which is consistent with late-stage biotite fractionation (K-
487 feldspar is interstitial to poikilitic in the WCb).

488 As with the lower zone, the major element mass balance calculations were also tested
489 using the REE. For crystal accumulation models, these calculations were similar to those for the
490 lower zone, in which REE abundances of hornblende, augite, plagioclase, biotite, and an
491 assumed melt were summed using proportions from the major element calculations. For each
492 test, one set of calculations used the composition of sample MMB-612 as the interstitial melt. A
493 second set used melt compositions calculated from hornblende, using partition coefficients from
494 Bachmann et al. (2005). Both proxies for melt composition result in close fits to the *shape* of the
495 bulk-rock REE pattern, although the fit to absolute abundances is variable (Fig. 7). Better fits can
496 be achieved by substituting different amphibole compositions and/or using different REE
497 partition coefficients; however, our goal here is to assess the viability of the models rather than
498 to achieve perfect fits. In that regard, it is noteworthy that although the two melt proxies are quite
499 distinct in their REE patterns and abundances, the results of trace element mass balance provide
500 close fits to the bulk-rock composition, an indication that the bulk-rock REE budget is dominated
501 by hornblende. In addition, although the cumulate minerals all have Eu anomalies, the calculated
502 REE patterns either lack Eu anomalies or have negligible ones (Fig. 7). Evidently, the presence

This is a preprint, the final version is subject to change, of the American Mineralogist (MSA)
Cite as Authors (Year) Title. American Mineralogist, in press.
(DOI will not work until issue is live.) DOI: http://dx.doi.org/10.2138/am-2016-5404

or absence of Eu anomalies may be an unreliable indicator of plagioclase fractionation or accumulation (cf. Deering and Bachmann, 2010).

Rare earth element mass balance tests of fractional crystallization attempted to match the composition of the presumed parent (MMB-612) to the sum of the fractionated melt (bulk-rock composition) plus fractionated crystals. The results (Fig. 8) show close fits to the REE patterns and abundances.

The relative proportions of cumulate minerals or residual melts are plotted on the geologic map (Fig. 1). Cumulate rocks occupy structurally lower parts of the upper zone (NE side; Fig. 9), whereas fractionated samples are in the structurally highest part of the zone. There is no discernable regular variation of the percentage of cumulate minerals among the cumulate rocks, or of the residual melt among the fractionated rocks. This lack of regular variation suggests that accumulation within the upper zone resulted from variable separation of melt from an initial andesitic magma (Fig. 9), leading to variable compositions of evolved magma in the uppermost parts of the system.

DISCUSSION

Lower zone. Aside from a few pyroxenite and melagabbro samples with adcumulate textures (Barnes, 1983; Coint et al., 2013b), most samples of the lower WCb lack structural or petrographic features that would identify them as cumulates in the sense of Wager and Brown (1968). Nevertheless, mineral compositions and mass balance calculations indicate that most lower-zone rocks are partial cumulates. If so, then the question arises: how did residual melts from lower-zone magmas separate from the cumulate minerals? We rule out crystal settling for a number of reasons, including the lack of field evidence and the fact that the lower zone formed

This is a preprint, the final version is subject to change, of the American Mineralogist (MSA)
Cite as Authors (Year) Title. American Mineralogist, in press.
(DOI will not work until issue is live.) DOI: http://dx.doi.org/10.2138/am-2016-5404

primarily by emplacement of multiple steeply-dipping, sheet-like bodies. In contrast, magma emplacement in sheet-like masses is consistent with accumulation due to flow sorting (e.g., Komar, 1972), particularly in the pyroxenite and melagabbro bodies. However, few of the bodies show inward increases in grain size, as would be expected if flow sorting were the primary mechanism of crystal accumulation. Some interstitial melts could escape due to a combination of hindered settling and compaction, but this process is more effective in horizontally-extensive tabular bodies (e.g., Bachmann and Bergantz, 2004).

We suggest that a more likely cause of expulsion of interstitial melts from lower-zone magmas was by deformation-induced filter pressing. Deformation was probably in part related to regional tectonic effects (e.g., Bea et al., 2005), which is consistent with the fact that magmatic foliation in the lower zone is subparallel to foliation in adjacent host rocks (Barnes, 1983; Coint et al., 2013b). In addition, growth of the lower zone by incremental emplacement of new magmas into existing, crystal-rich magmas would have resulted in compaction of existing mushy magmas and expulsion of interstitial melts. The latter process explains the highly variable calculated proportions of cumulate minerals in the pyroxenite–diorite group, because the types and proportions of cumulate minerals would be dependent on phenocryst assemblage at the time of filter pressing. The phenocryst assemblage would, in turn, depend on the T and H_2O content of the melt: higher T and H_2O content would result in suppression of plagioclase stability and therefore pyroxenitic–melagabbroic cumulate rocks, whereas lower T and/or lower H_2O content would promote plagioclase stability and formation of gabbroic to dioritic cumulate rocks.

In contrast to the pyroxenite–diorite group, the ratios of cumulate plagioclase/(plagioclase + pyroxene) in the quartz diorite–tonalite group are quite uniform, and this plagioclase/pyroxene proportion is similar to the plagioclase/(plagioclase + pyroxene) ratio

This is a preprint, the final version is subject to change, of the American Mineralogist (MSA)
Cite as Authors (Year) Title. American Mineralogist, in press.
(DOI will not work until issue is live.) DOI: http://dx.doi.org/10.2138/am-2016-5404

549 determined from rhyolite-MELTS models at temperatures of 950–1000°C and low to moderate
550 H_2O contents. Evidently, in the case of the quartz diorite–tonalite group, deformation-induced
551 filter pressing preserved a cumulate assemblage that closely mimicked cotectic mineral
552 proportions. As a result, the compositional trends within this group (Fig. 3) are best interpreted
553 as accumulation trends rather than as liquid lines of descent. Inasmuch as rocks in this group
554 generally have moderate to strong magmatic foliation defined by oriented plagioclase, loss of
555 melt by deformation-induced filter pressing at temperatures somewhat lower than 950°C.
556 Upper zone. Changes in slope of the compositional trends for the upper zone are characteristic of
557 fractional crystallization. However, the uniformity of hornblende compositions (Coint et al.,
558 2013a) and plagioclase core compositions (Fig. 2A; Barnes, 1987) indicate that the crystal-liquid
559 separation in the upper zone was inefficient. Moreover, the mass balance calculations are entirely
560 consistent with zonation within the upper zone caused by separation of melt from a cumulate
561 assemblage that closely approached a plagioclase/(plagioclase + mafic mineral) ratio of 0.47
562 (Table 4). In this interpretation, the melt phase in a nominally homogeneous upper-zone magma
563 body was able to rise to structurally high levels of the batholith, leaving partial cumulates
564 behind. This process requires that a melt-rich zone as much as 1.35 km thick formed from an
565 upper-zone magma body that was as much as 4 km thick. For this separation to occur, magma
566 properties must be appropriate for a process such as hindered settling to occur.
567 In a recent contribution, Lee et al. (2015) calculated conditions necessary for hindered
568 settling and compaction to result in crystal-melt separation over geologically reasonable times.
569 These calculations utilized porosity (~melt fraction), melt viscosity, density difference between
570 crystalline assemblage and melt, crystal size, and time as variables. We used the results of mass

This is a preprint, the final version is subject to change, of the American Mineralogist (MSA)
Cite as Authors (Year) Title. American Mineralogist, in press.
(DOI will not work until issue is live.) DOI: http://dx.doi.org/10.2138/am-2016-5404

balance calculations to estimate porosity and output from rhyolite-MELTS simulations to estimate magma properties for comparison with the calculations of Lee et al. (2015).

Melt viscosity was calculated at 850°C for the compositions of sample MMB-612 and of differentiated melt compositions from rhyolite-MELTS output. The method of Giordano et al. (2008) yields $\log_{10}$ melt viscosities in the range of 4.1 to 4.9 Pa sec. At 850°C, rhyolite-MELTS calculations indicate density differences between melt and solids of 600–700 kg/m^3. If the mass balance results are taken to approximate porosity, then porosity ranged from 0.8 to 0.37, with most values >0.55.

The results of Lee et al. (2015) indicate that for porosity of 0.55, solid/melt density difference of 300 kg/m^3, crystal diameter of 3mm, and $\log_{10}$ melt viscosity of 5 Pa sec, a 500m-thick differentiated 'boundary layer' can form in ~30 kyr by hindered settling and ~50 kyr by compaction. The models of Lee et al. (2015) assume no addition of heat during crystal-melt separation. However, zones of mixing/mingling are common at the base of the upper zone. If these magma influxes provided heat to the upper zone magma, then it is likely that sufficient time was available for formation of the ca. 1.35 km thick fractionated zone.

IMPLICATIONS

On the basis of textural and bulk-rock compositional data, mineral–bulk-rock Fe-Mg K(d) data, major element mass balance calculations, and rhyolite-MELTS simulations, we conclude that the great majority of rocks in the WCb are cumulate. Only the uppermost part of the batholith represents differentiated magmas, and these rocks are interpreted to result from upward percolation of melts in a magmatic mush. Among the most mafic lower zone rocks, the total mass of cumulate minerals varies widely, as do the proportions of cumulate minerals. In contrast, with increasing SiO_2 content of the magmas, the percentage of trapped melt tends to be

more uniform, as do the proportions of cumulate minerals. This consistency of cumulate mineral proportions results from accumulation in near-cotectic proportions and leads to bulk-rock compositional trends that mimic liquid lines of descent.

If the type of accumulation seen in the WCb is typical of arc plutons, then direct comparison of plutonic rock compositions with volcanic rock compositions will result in the observation that plutons are more mafic than coeval volcanic rocks (e.g., Lee and Morton, 2015). Our results indicate that such comparisons should be made with caution, and that the expectation that direct comparison between volcanic and plutonic suites will yield identical compositional ranges is probably unrealistic. Instead, we suggest that wherever possible mineral–bulk-rock Fe-Mg K(d) values should be used to assess the likelihood of accumulation. Inasmuch as hornblende is the common ferromagnesian silicate in many arc plutons, further research on refining the range of mineral–melt K(d) values for calcic amphibole is highly desirable.

ACKNOWLEDGEMENTS

We thank reviewers Chad Deering and Drew Coleman and Associate Editor Calvin Miller for helpful comments. This research was supported by NSF grant EAR-0838342 to Yoshinobu and Barnes and a Geological Society of America Penrose grant to Coint.

REFERENCES CITED

Annen, C., Blundy, J.D., and Sparks, R.S.J. (2006) The genesis of intermediate and silicic magmas in deep crustal hot zones. Journal of Petrology, 47, 505–539.

Bachmann, O., and Bergantz, G.W. (2004) On the origin of crystal-poor rhyolites: Extracted from batholithic crystal mushes. Journal of Petrology, 45, 1565–1582.

616 Bachmann, O., Dungan, M.A., and Bussy, F. (2005) Insights into shallow magmatic processes in
617 large silicic magma bodies: the trace element record in the Fish Canyon magma body,
618 Colorado. Contributions to Mineralogy and Petrology, 149, 338–349.
619 Bachmann, O., Oberli, F., Dungan, M.A., Meier, M., Mundil, R., and Fischer, H. (2007)
620 $^{40}Ar/^{39}Ar$ and U–Pb dating of the Fish Canyon magmatic system, San Juan Volcanic
621 filed, Colorado: Evidence for an extended crystallization history. Chemical Geology, 236,
622 134–166.
623 Barnes, C.G. (1983) Petrology and upward zonation of the Wooley Creek batholith, Klamath
624 Mountains, California. Journal of Petrology, 24, 495–537.
625 Barnes, C.G. (1987) Mineralogy of the Wooley Creek batholith, Slinkard pluton, and related
626 dikes, Klamath Mountains, northern California. American Mineralogist, 72, 879–901.
627 Barnes, C.G., Allen, C.M., and Saleeby, J.B. (1986a) Open- and closed-system characteristics of
628 a tilted plutonic system, Klamath Mountains, California. Journal of Geophysical
629 Research, 91, 6073–6090.
630 Barnes, C.G., Rice, J.M., and Gribble, R.F. (1986b) Tilted plutons in the Klamath Mountains of
631 California and Oregon. Journal of Geophysical Research, 91, 6059–6071.
632 Barnes, C.G., Allen, C.M., Hoover, J.D., & Brigham, R.H. (1990) Magmatic components of a
633 tilted plutonic system, Klamath Mountains, California. In Anderson, J.L., Ed., The nature
634 and origin of Cordilleran magmatism. Geological Society of America Memoir, 174, 331–
635 346.
636 Barnes, C.G., Johnson, K., Barnes, M.A., Prestvik, T., Kistler, R.W., and Sundvoll, B. (1995)
637 The Grayback pluton: Magmatism in a Jurassic back-arc environment, Klamath
638 Mountains, Oregon. Journal of Petrology, 36, 397–416.

639 Barnes C.G., Mars, E.V., Swapp, S., and Frost, C.D. (2006) Evolution of potassic magmas in a
640 primitive arc setting. In Snoke, A.W. and Barnes, C.G., Eds, Geological studies in the
641 Klamath Mountains province, California and Oregon: A volume in honor of William P.
642 Irwin. Geological Society of America Special Paper, 410, 199–221.
643 Beane, R., and Wiebe, R.A. (2012) Origin of quartz clusters in Vinalhaven granite and porphyry,
644 coastal Maine. Contributions to Mineralogy and Petrology, 163, 1069–1082.
645 Beard, J.S. (1986) Characteristic mineralogy of arc-related cumulate gabbros: Implications for
646 the tectonic setting of gabbroic plutons and for andesite genesis. Geology, 14, 848–851.
647 Bédard, J.H., Leclerc, F., Harris, L.B., and Gulet, N. (2009) Intra-sill magmatic evolution in the
648 Cummings Complex, Abitibi greenstone belt: Tholeiitic to calc-alkaline magmatism
649 recorded in an Archaean subvolcanic conduit system. Lithos, 111, 47–71.
650 Bowen, N.L (1928) The evolution of the igneous rocks. Princeton Univ. Press, 334 p.
651 Bryan, W. B., Finger, L. W., and Chayes, F. (1969) Estimating proportions in petrographic
652 mixing equations by least-squares approximation. Science, 163, 163–164.
653 Burgisser, A., and Bergantz, G.W. (2011) A rapid mechanism to remobilize and homogenize
654 highly crystalline magma bodies. Nature, 471, 212–217.
655 Clemens, J.D., Helps, P.A., and Stevens, G. (2010) Chemical structure in granitic magmas – a
656 signal from the source?: Earth and Environmental Science Transactions of the Royal
657 Society of Edinburgh, 100, 159–172.
658 Coint, N., Barnes, C.G., Yoshinobu, A.S., Barnes, M.A., and Buck, S. (2013a) Use of trace
659 element abundances in augite and hornblende to determine the size, connectivity, timing,
660 and evolution of magma batches in a tilted pluton. Geosphere, 9, 1747–1765.

661 Coint, N., Barnes, C.G., Yoshinobu, A.S., Chamberlain, K.R., and Barnes, M.A. (2013b) Batch-
662 wise assembly and zoning of a tilted calc-alkaline batholith: Field relations, timing, and
663 compositional variation. Geosphere, 9, 1729–1746.
664 Coleman, D.S., Bartley, J.M., Glazner, A.F., and Pardue, M.J. (2012) Is chemical zonation in
665 plutonic rocks driven by changes in source magma composition or shallow-crustal
666 differentiation? Geosphere, 8, 1568–1587.
667 Darwin, C. (1844) Geological observations on the volcanic islands visited during the voyage of
668 the HMS Beagle, together with some notes on the geology of Australia and the Cape of
669 Good Hope, being the second part of the geology of the voyage of the Beagle, under the
670 command of Capt. Fitzroy, R.N., during the years 1832 to 1836. Smith Elder, London.
671 Daly, R.A. (1933) Igneous Rocks and the Depths of the Earth. New York, McGraw-Hill, 598 p.
672 Deering, C.D., and Bachmann, O. (2010) Trace element indicators of crystal accumulation in
673 silicic igneous rocks. Earth and Planetary Science Letters, 297, 324–331.
674 Donato, M.M., Barnes, C.G., and Tomlinson, S.L. (1996) The enigmatic Applegate Group of
675 southwestern Oregon: Age, correlation, and tectonic affinity. Oregon Geology, 58, 79–
676 91.
677 du Bray, E.A., Bacon, C.R., John, D.A., Wooden, J.L., and Mazdab, F.K. (2011) Episodic
678 intrusion , internal differentiation, and hydrothermal alteration of the Miocene Tatoosh
679 intrusive suite south of Mount Rainier, Washington. Geological Society of America
680 Bulletin, 123, 534–561.
681 Flood, R.H., and Shaw, S.E. (1979) K-rich cumulate diorite at the base of a tilted granodiorite
682 pluton from the New England batholith, Australia. Journal of Geology, 87, 417–425.

683 Gelman, S.E., Deering, C.D., Bachmann, O., Huber, C., and Gutiérrez, F.J. (2014) Identifying
684 the crystal graveyards remaining after large silicic eruptions. Earth and Planetary Science
685 Letters, 403, 299–306.
686 Gillluly, J. (chairman) (1948) Origin of granites. Geological Society of America, Memoir 28,
687 139p.
688 Glazner, A.F., Coleman, D.S., and Mills, R.D. (2015) The volcanic-plutonic connection.
689 Advances in Volcanology, Springer Berlin Heidelberg, 1–22, doi:
690 10.1007/11157_2015_11.
691 Gray, G.G. (1986) Native terranes of the central Klamath Mountains, California. Tectonics, 5,
692 1043–1054.
693 Grunder, A.L., Klemetti, E.W., Feeley, T.C., and McKee, C.M. (2006) Eleven million years of
694 arc volcanism at the Aucanquilcha Volcanic Cluster, northern Chilean Andes:
695 implications for the life span and emplacement of plutons. Transactions of the Royal
696 Society of Edinburgh: Earth Sciences, 97, 415–436.
697 Gualda, G.A.R., and Ghiorso, M.S. (2014) Phase-equilibrium geobarometers for silicic rocks
698 based on rhyolite-MELTS. Part 1.: Principles, procedures, and evaluation of the method.
699 Contributions to Mineralogy and Petrology, 168, http://dx.doi.org/10.1007/s00410-014-
700 1033-3.
701 Gualda, G.A.R., and Ghiorso, M.S. (2015) MELTS_Excel: A Microsoft Excel-based MELTS
702 interface for research and teaching of magma properties and evolution. Geochemistry
703 Geophysics Geosystems, 16, http://dx.doi.org/10.1002/2014GC005545

704 Hacker, B.R., Donato, M.M., Barnes, C.G., McWilliams, M.O., and Ernst, W.G. (1995)
705 Timescales of orogeny: Jurassic construction of the Klamath Mountains. Tectonics, 14,
706 677–703, doi: 10.1029/94TC02454.
707 Harper, B.E., Miller, C.F., Koteas, G.C., Cates, N.L., Wiebe, R.A., Lazzareschi, D.S., and Cribb,
708 J.W. (2004) Granites, dynamic magma chamber processes and pluton construction: the
709 Aztec Wash pluton, Eldorado Mountains, Nevada, USA. Transactions of the Royal
710 Society of Edinburgh: Earth Sciences, 95, 277–295.
711 Hildreth, W. (2004) Volcanological perspectives on Long Valley, Mammoth Mountain, and
712 Mono Craters: several contiguous but discrete systems. Journal of Volcanology and
713 Geothermal Research, 136, 169–198.
714 Hildreth, W., and Moorbath, S. (1988) Crustal contributions to arc magmatism in the Andes of
715 central Chile. Contributions to Mineralogy and Petrology, 98, 455–489.
716 Hunter, R. (1996) Texture development in cumulate rocks, In Cawthorn, R., Ed., Layered
717 Intrusions, Elsevier Sciences B.V., p. 77–101.
718 Irwin, W.P. (1960) Geologic reconnaissance of the northern Coast Ranges and Klamath
719 Mountains, California, with a summary of the mineral resources. San Francisco,
720 California Division of Mines Bulletin 179, 80 p.
721 Irwin, W.P. (1972) Terranes of the Western Paleozoic and Triassic belt in the southern Klamath
722 Mountains, California. U.S. Geological Survey Professional Paper, 800-C, 103–111.
723 Jachens, R.C., Barnes, C.G., and Donato, M.M. (1986) Subsurface configuration of the Orleans
724 fault: Implications for deformation in the western Klamath Mountains, California.
725 Geological Society of America Bulletin, 97, 388–395.

726 Keller, C.B., Schoene, B., Barboni, M., Samperton, K.M., and Husson, J.M. (2015) Valcanic–
727 plutonic parity and the differentiation of the continental crust. Nature, 523, 301–307.
728 Komar, P.D. (1972) Flow differentiation of igneous dikes and sills: Profiles of velocity and
729 phenocryst concentration. Geological Society of America Bulletin, 83, 973–988.
730 Lee, C.-T.A., and Morton, D.M. (2015) High silica granites: Terminal porosity and crystal
731 settling in shallow magma chambers. Earth and Planetary Science Letters, 409, 23–31.
732 Lee, C.-T.A., Morton, D.M., Farner, M.J., and Moitra, P. (2015) Field and model constraints on
733 silicic melt segregation by compaction/hindered settling: the role of water and its effect
734 on latent heat release. American Mineralogist, 100, 1762–1777.
735 Lipman, P.W., and Bachmann, O. (2015) Ignimbrites to batholiths: Integrating perspectives from
736 geological, geophysical, and geochronological data. Geosphere, 11,
737 doi:10.1130/GES01091.1.
738 Lux, D.R., Hooks, B., Gibson, D., and Hogan, J.P. (2007) Magma interactions in the Deer Isle
739 granite complex, Maine: Field and textural evidence. The Canadian Mineralogist, 45,
740 131–146.
741 Miller, C.F., and Miller, J.S. (2002) Contrasting stratified plutons exposed in tilt blocks,
742 Eldorado Mountains, Colorado River rift, NV, USA. Lithos, 61, 209–224.
743 Miller, C.F., Furbish, D.J., Walker, B.A., Claiborne, L.L., Koteas, G.C., Bleick, H.A., and
744 Miller, J.S. (2011) Growth of plutons by incremental emplacement of sheets in crystal-
745 rich host: Evidence from Miocene intrusions of the Colorado River region, Nevada, USA.
746 Tectonophysics, 500, 65–77.

747 Mills, R.D., and Coleman, D.S. (2013) Temporal and chemical connections between plutons and
748 ignimbrites from the Mount Princeton magmatic center. Contributions to Mineralogy and
749 Petrology, 165, 961–980.
750 Mills, R.D., Coleman, D.S., Frazer, R.E., Glazner, A.F., and Tappa, M.J. (2012) The general lack
751 of igneous rocks with cumulate chemical signatures: is there an elephant in the room?
752 Abstract V43D-2893 presented at 2012 Fall Meeting, AGU, San Francisco, Calif., 3-7
753 Dec.
754 Naney, M.T. (1983) Phase equilibria of rock-forming ferromagnesian silicates in granitic
755 systems. American Journal of Science, 283, 993-1033.
756 Naslund, H., and McBirney, A. (1996) Mechanisms of formation of igneous layering, In
757 Cawthorn, R., Ed., Layered Intrusion, Elsevier Science B.V., 1-41.
758 Paterson, S.R. (2009) Magmatic tubes, pipes, troughs, diapirs, and plumes: Late-stage convective
759 instabilities resulting in compositional diversity and permeable networks in crystal-rich
760 magmas of the Tuolumne batholith, Sierra Nevada, California. Geosphere, 5, 1–32.
761 Putirka, K. (2008) Thermometers and Barometers for Volcanic Systems. In: Putirka, K., Tepley,
762 F., Eds., Minerals, Inclusions and Volcanic Processes, Reviews in Mineralogy and
763 Geochemistry, Mineralogical Society of America, 69, 61–120.
764 Reubi, O., and Blundy, J. (2009) A dearth of intermediate melts at subduction zone volcanoes
765 and the petrogenesis of arc andesites. Nature, 461, 1269–1274.
766 Ruprecht, P., Bergantz, G.W., Cooper, K.M., and Hildreth, W. (2012) The crustal magma storage
767 system of Volcán Quizapu, Chile, and the effects of magma mixing on magma diversity.
768 Journal of Petrology, 53, 801–840.

769 Sawka, W.N., Chappell, B.W., and Kistler, R.W. (1990) Granitoid compositional zoning by side-
770 wall boundary layer differentiation: Evidence from the Palisade Crest intrusive suite,
771 central Sierra Nevada, California. Journal of Petrology, 31, 519-553.
772 Singer, B.S., Andersen, N.L., Le Mével, H., Feigl, K.L., DeMets, C., Tikoff, B., Thurber, C.H.,
773 Jicha, B.R., Cardona, C., Códova, L., Gil, F., Unsworth, M.J., Williams-Jones, G., Miller,
774 C.F., Fierstein, J., Hildreth, W., and Vazquez, J. (2014) Dynamics of a large, restless,
775 rhyolitic magma system at Laguna del Maule, southern Andes, Chile. GSA Today, 24, 4–
776 10.
777 Snoke, A. W. and Barnes C. G. (2006) The development of tectonic concepts for the Klamath
778 Mountains province, California and Oregon. In Snoke, A.W. and Barnes, C.G., Eds,
779 Geological studies in the Klamath Mountains province, California and Oregon: A volume
780 in honor of William P. Irwin. Geological Society of America Special Paper, 410, 1–29.
781 Srogi, L., and Lutz, T.M. (1996) The role of residual melt migration in producing compositional
782 diversity in a suite of granitic rocks. Earth and Planetary Science Letters, 144, 563–576.
783 Srogi, L., and Lutz, T.M. (1997) Chemical variation in plutonic rocks caused by residual melt
784 migration: Implications for granite petrogenesis, In Sinha, A.K., Whalen, J.B., and
785 Hogan, J.P., Eds., The nature of magmatism in the Appalachian Orogen, Volume 191:
786 Geological Society of America Memoir, 191 309–335.
787 Tappa, M.J., Coleman, D.S., Mills, R.D., and Samperton, K.M. (2011) The plutonic record of a
788 silicic ignimbrite from the Latir volcanic field, New Mexico. Geochemistry Geophysics
789 Geosystems, 12, doi: 10.1029/2011GC003700.

790 Vernon, R.H., and Paterson, S.R. (2008) Mesoscopic structures resulting from crystal
791 accumulation and melt movement in granites. Transactions of the Royal Society of
792 Edinburgh: Earth Sciences, 97,369–381.
793 Wager, L.R., and Brown, G.M. (1968) Layered igneous rocks. Edinburgh. Oliver and Boyd, 588
794 p.
795 Wager, L.R., Brown, G.M., and Wadsworth, W.J. (1960) Types of igneous cumulates. Journal of
796 Petrology, 1, 73–85.
797 Wiebe, R., and Collins, W. (1998) Depositional features and stratigraphic sections in granitic
798 plutons: implications for the emplacement and crystallization of granitic magma. Journal
799 of Structural Geology, 20, 1273–1289.
800 Wright, J.E. (1982) Permo-Triassic accretionary subduction complex, southwestern Klamath
801 Mountains, northern California. Journal of Geophysical Research, 87, 3805–3818.
802 Wright, J.E., and Fahan, M.R. (1988) An expanded view of Jurassic orogenesis in the western
803 United States Cordillera: Middle Jurassic (pre-Nevadan) regional metamorphism and
804 thrust faulting within an active arc environment, Klamath Mountains, California.
805 Geological Society of America Bulletin, 100, 859–876.
806 Wright, J.E., and Wyld, S.J. (1994) The Rattlesnake Creek terrane, Klamath Mountains,
807 California: An early Mesozoic volcanic arc and its basement of tectonically disrupted
808 oceanic crust. Geological Society of America Bulletin, 106, 1033–1056.
809
810 FIGURE CAPTIONS
811

This is a preprint, the final version is subject to change, of the American Mineralogist (MSA)
Cite as Authors (Year) Title. American Mineralogist, in press.
(DOI will not work until issue is live.) DOI: http://dx.doi.org/10.2138/am-2016-5404

Figure 1. Map of Wooley Creek batholith showing sample locations, rock types, and zone boundaries. The upper zone is divided into the structurally lower part with partial cumulate rocks and the structurally higher part with differentiated rocks. Numbers adjacent to sample locations in the 'upper zone cumulates' region indicate calculated proportion of intergranular melt. Numbers adjacent to sample locations in the 'upper zone differentiates' region represent the differentiated melt fraction represented by the rock. Inset shows the location of the batholith in the Klamath Mountain geologic province.

Figure 2. Mineral compositions. A. Ranges of plagioclase compositions in the batholith. The central tic mark indicates average plagioclase composition for each sample. For lower zone samples, blue symbols are plagioclase from the pyroxenite–diorite group and green symbols are for plagioclase from the quartz diorite–tonalite group. B. Pyroxene quadrilateral. C. Rare earth element patterns of augite from selected lower zone samples. Fields indicate the ranges of augite compositions in individual samples except for tonalite sample MMB-30, for which the range of REE patterns encompasses nearly the entire range of the other three samples.

Figure 3. A–D are variations diagrams of MgO (A), Na_2O (B), TiO_2 (C), and Sr (D) of bulk rocks, pyroxenes, hornblende, and plagioclase plotted versus SiO_2 for rocks of the lower and central zones. Compositions of mafic synplutonic dikes are plotted in (A) but not shown in the other diagrams. The star symbols represent samples used in mass balance calculations and are labelled according to sample number. Blue stars indicate interstitial melt compositions used in lower zone pyroxenite–diorite calculations, green stars indicate interstitial melt used in lower zone quartz diorite–tonalite calculations. (E) The curves represent the range of $K(d)_{Fe\text{-}Mg}$

This is a preprint, the final version is subject to change, of the American Mineralogist (MSA)
Cite as Authors (Year) Title. American Mineralogist, in press.
(DOI will not work until issue is live.) DOI: http://dx.doi.org/10.2138/am-2016-5404

equilibrium values [$(K(d)_{Fe\text{-}Mg} = (Mg_{rock})*(Fe_{pyroxene})/(Mg_{pyroxene})*(Fe_{rock})$] indicating equilibrium between opx and its host melt (after Putirka, 2008). (F) Observed clinopyroxene components plotted against components predicted on the basis of their host bulk-rock compositions (Putirka, 2008).

Figure 4. Variation diagrams for upper zone rocks. The star symbol represents sample MMB-612, which was used as a potential parental composition to the upper zone. The arrow is the inferred liquid line of descent from the parent, whereas samples with SiO_2 contents lower than MMB-612 are interpreted to be partial cumulates.

Figure 5. Summary of mass balance calculations of lower zone samples. Percent melt is plotted against mass percentages of augite, opx, and plagioclase.

Figure 6. Rare earth element tests of lower-zone mass balance calculations. Calculations were based on the results of major element mass balance and compositions of augite, orthopyroxene, and plagioclase. Two compositions of interstitial melt were used: the bulk-rock composition of the 'melt' used in major element models (gray squares) and the REE of melt calculated to be in equilibrium with augite (pink squares). Green squares are REE patterns of the bulk rock composition to be matched. A. Match to diorite WCB-152. B. Match to tonalite WCB-156. C and D. Match to tonalite MMB-30, in which REE concentrations in augite vary over more than 1.5 orders of magnitude. In C, the calculated melt used a high-REE value, but in D the average REE content of augite was used.

This is a preprint, the final version is subject to change, of the American Mineralogist (MSA)
Cite as Authors (Year) Title. American Mineralogist, in press.
(DOI will not work until issue is live.) DOI: http://dx.doi.org/10.2138/am-2016-5404

Figure 7. Rare earth element tests of upper-zone accumulation mass balance calculations. Calculations were based on the results of major element mass balance and compositions of hornblende, augite, biotite, and plagioclase. Two compositions of interstitial melt were used: the bulk-rock composition of the 'melt' used in major element models (MMB-612; orange squares) and the REE of melt calculated to be in equilibrium with hornblende (red squares). Yellow circles are REE patterns of the bulk rock composition to be matched. A. Match to biotite hornblende tonalite MMB-379. B. Match to biotite hornblende tonalite MMB-687. C. Match to biotite hornblende quartz diorite MMB-318.

Figure 8. Rare earth element tests of upper-zone fractional crystallization mass balance calculations. Calculations were based on the results of major element mass balance and compositions of hornblende, biotite, and plagioclase. The compositions of the 'daughter' melt (bulk rock composition) were added to mineral composition in an attempt to match the potential parental magma (MMB-612; pink triangles). A. Match to biotite hornblende granite MMB-372A. B. Match to biotite hornblende granodiorite MMB-361. Match to biotite hornblende granodiorite MMB-320.

Figure 9. Cartoon of emplacement and evolution of upper zone magmas. A. The upper zone is constructed from pyroxene hornblende andesite, with overall composition similar to MMB-612, examples of which are preserved as 'roof-zone' dikes. Basaltic magmas were emplaced into and through the central zone and ponded at the base of the upper zone, forming zones of pillowed mafic enclaves. Heat from these mafic magmas drove convection of upper zone magmas, effectively mixing any distinct magma batches and entraining and dispersing mafic enclaves. B.

This is a preprint, the final version is subject to change, of the American Mineralogist (MSA)
Cite as Authors (Year) Title. American Mineralogist, in press.
(DOI will not work until issue is live.) DOI: http://dx.doi.org/10.2138/am-2016-5404

Subsequent cooling and crystallization of upper zone magmas resulted in accumulation of hornblende and plagioclase ± biotite in structurally lower parts of the zone as residual melt-rich magmas migrated upward.

TABLES

Table 1. Trace element abundances in WCb plagioclase.

Table 2. Representative input to mass balance calculations.

Table 3. Mass balance results for lower zone.

Table 4. Mass balance results for upper zone.

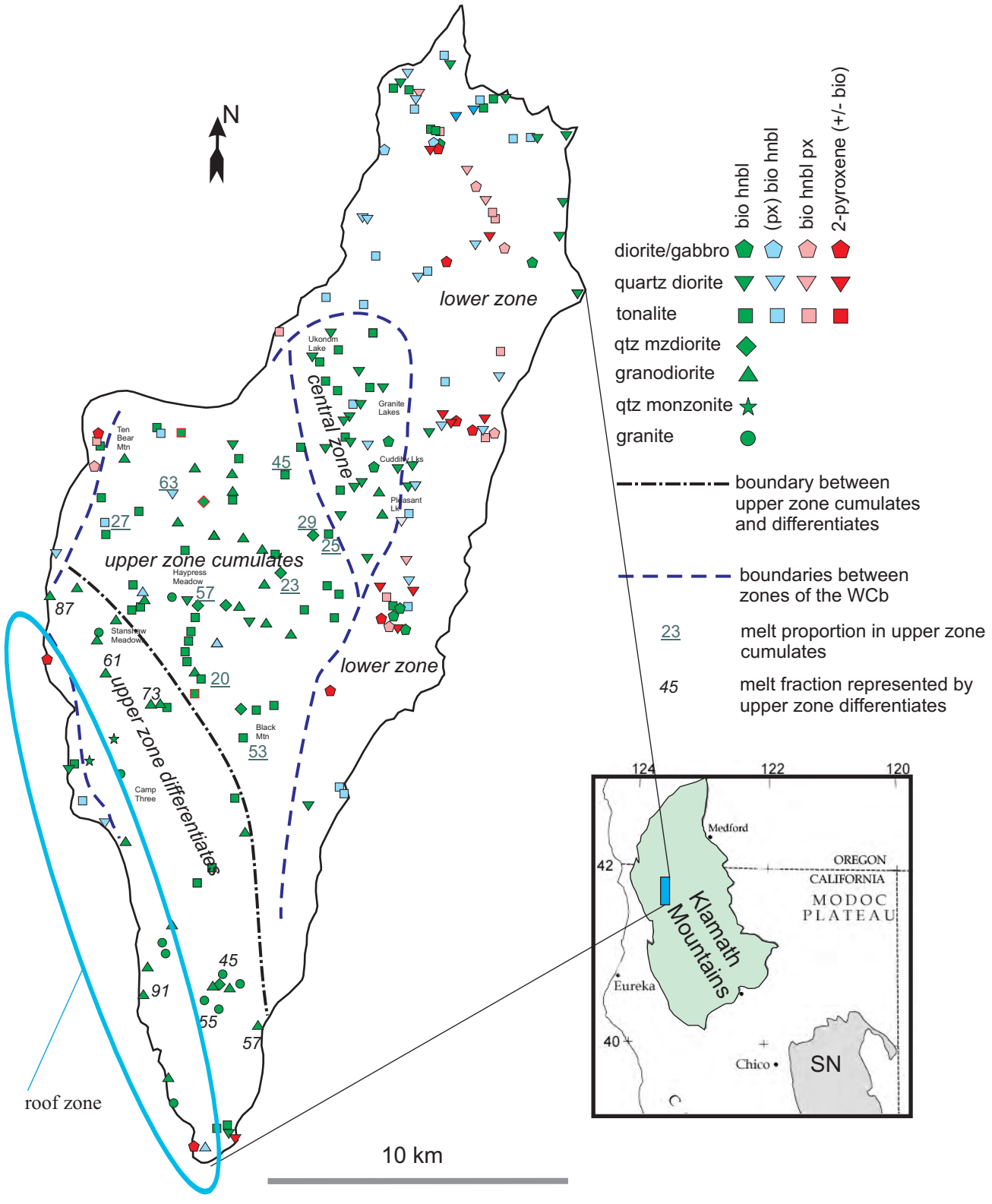
N
lower zone
central zone
upper zone cumulates
lower zone
upper zone differentiates
roof zone
Ukonom Lake
Granite Lakes
Ten Bear Mtn
Haypress Meadow
Stanshaw Meadow
Black Mtn
Camp Three
87
61
73
63
27
45
29
25
23
57
20
53
45
91
55
57
bio hnbl
(px) bio hnbl
bio hnbl px
2-pyroxene (+/- bio)
diorite/gabbro
quartz diorite
tonalite
qtz mzdiorite
granodiorite
qtz monzonite
granite
boundary between upper zone cumulates and differentiates
boundaries between zones of the WCb
23
melt proportion in upper zone cumulates
45
melt fraction represented by upper zone differentiates
124
122
120
42
40
Medford
OREGON
CALIFORNIA
MODOC PLATEAU
Klamath Mountains
Eureka
Chico
SN
10 km

Figure 1

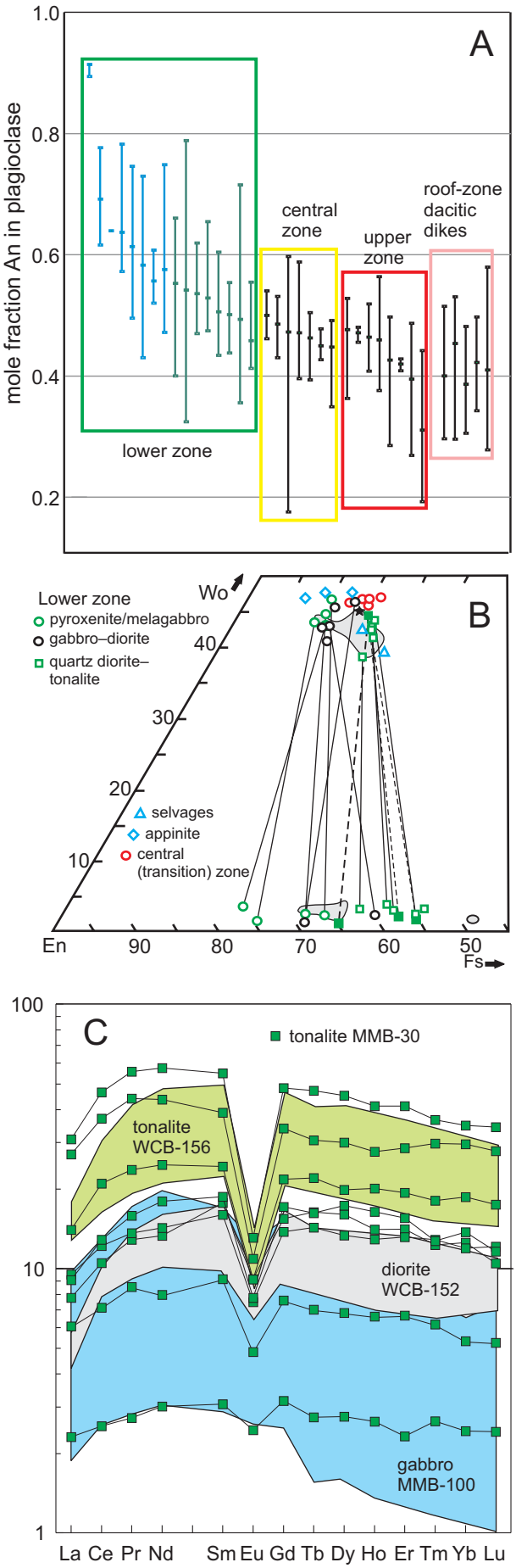
A
mole fraction An in plagioclase
1.0
0.8
0.6
0.4
0.2
lower zone
central zone
upper zone
roof-zone dacitic dikes
B
Lower zone
pyroxenite/melagabbro
gabbro–diorite
quartz diorite–tonalite
selvages
appinite
central (transition) zone
Wo
40
30
20
10
En
90
80
70
60
50
Fs
C
tonalite MMB-30
tonalite WCB-156
diorite WCB-152
gabbro MMB-100
100
10
1
La Ce Pr Nd Sm Eu Gd Tb Dy Ho Er Tm Yb Lu

Figure 2

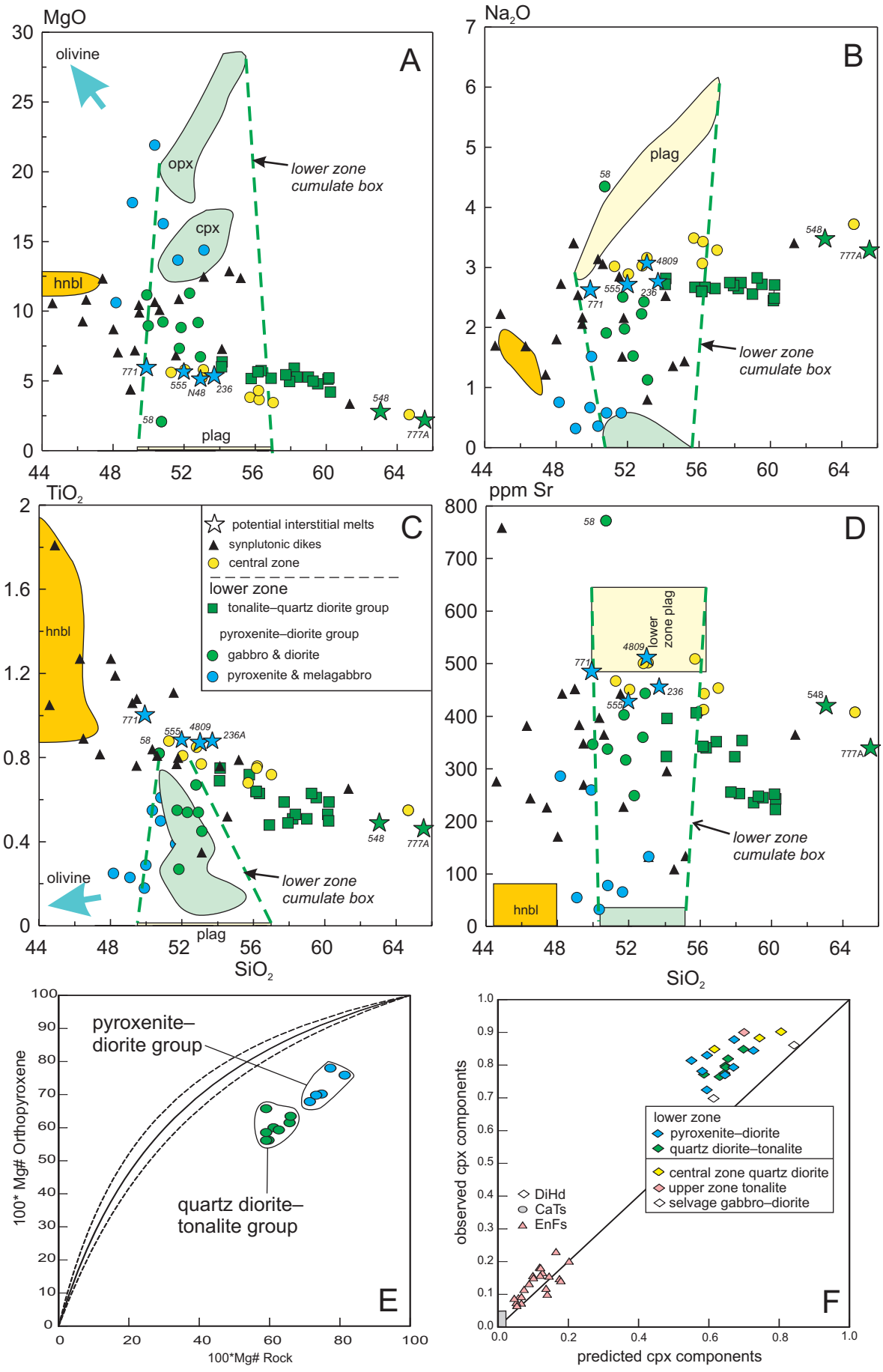
MgO
A
olivine
opx
cpx
hnbl
plag
lower zone
cumulate box
Na2O
B
plag
lower zone
cumulate box
TiO2
C
potential interstitial melts
synplutonic dikes
central zone
lower zone
tonalite–quartz diorite group
pyroxenite–diorite group
gabbro & diorite
pyroxenite & melagabbro
hnbl
olivine
plag
lower zone
cumulate box
SiO2
ppm Sr
D
lower zone plag
hnbl
lower zone
cumulate box
SiO2
pyroxenite–
diorite group
quartz diorite–
tonalite group
100* Mg# Orthopyroxene
100*Mg# Rock
E
observed cpx components
predicted cpx components
lower zone
pyroxenite–diorite
quartz diorite–tonalite
central zone quartz diorite
upper zone tonalite
selvage gabbro–diorite
DiHd
CaTs
EnFs
F

Figure 3

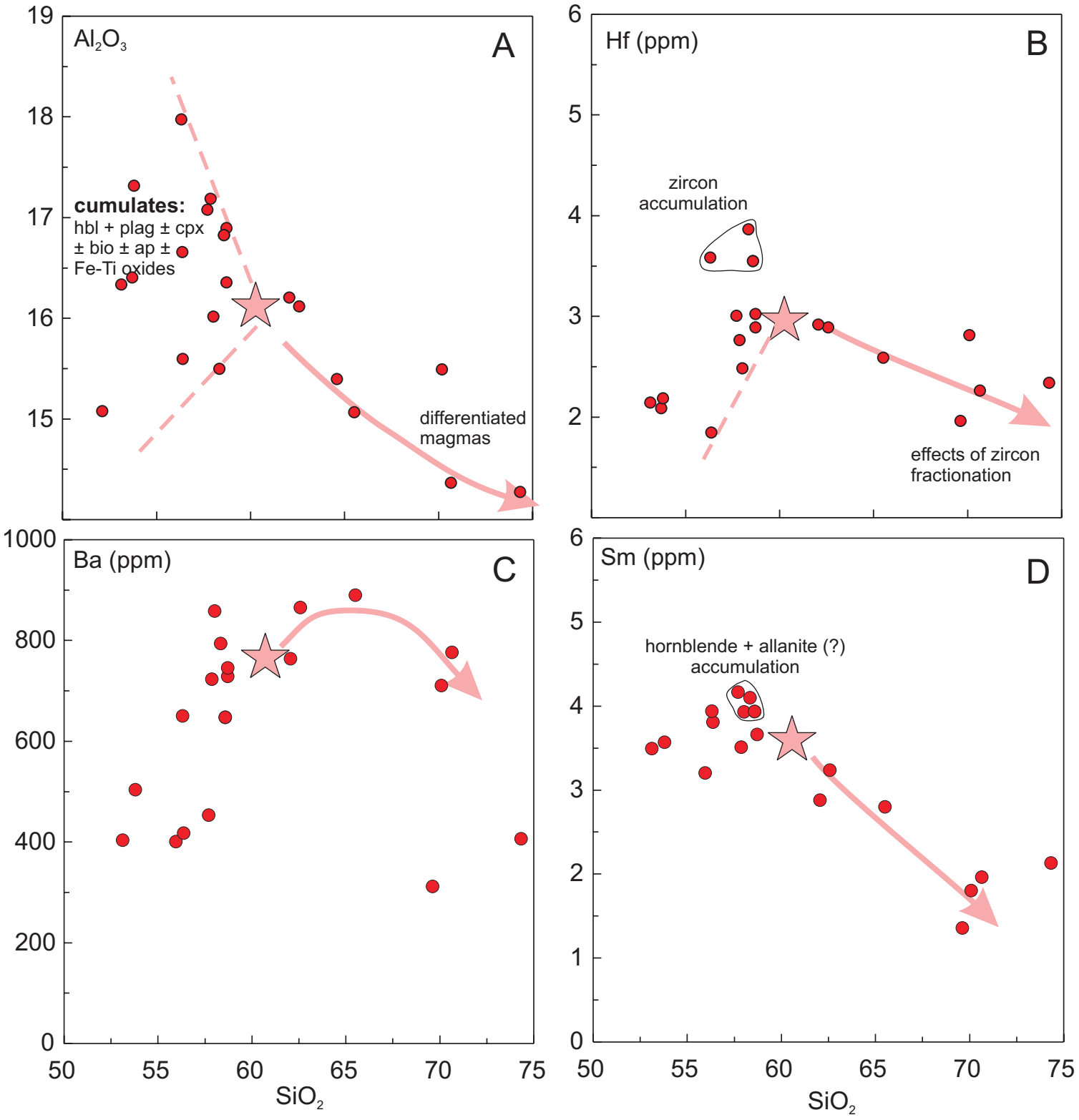
A
Al_2O_3
cumulates:
hbl + plag ± cpx
± bio ± ap ±
Fe-Ti oxides
differentiated
magmas
B
Hf (ppm)
zircon
accumulation
effects of zircon
fractionation
C
Ba (ppm)
D
Sm (ppm)
hornblende + allanite (?)
accumulation
SiO_2
SiO_2

Figure 4

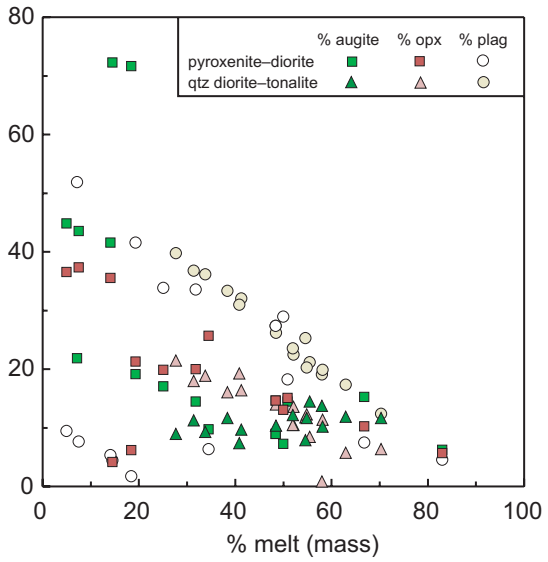
% augite
% opx
% plag
pyroxenite–diorite
qtz diorite–tonalite
80
60
40
20
0
0
20
40
60
80
100
% melt (mass)

Figure 5

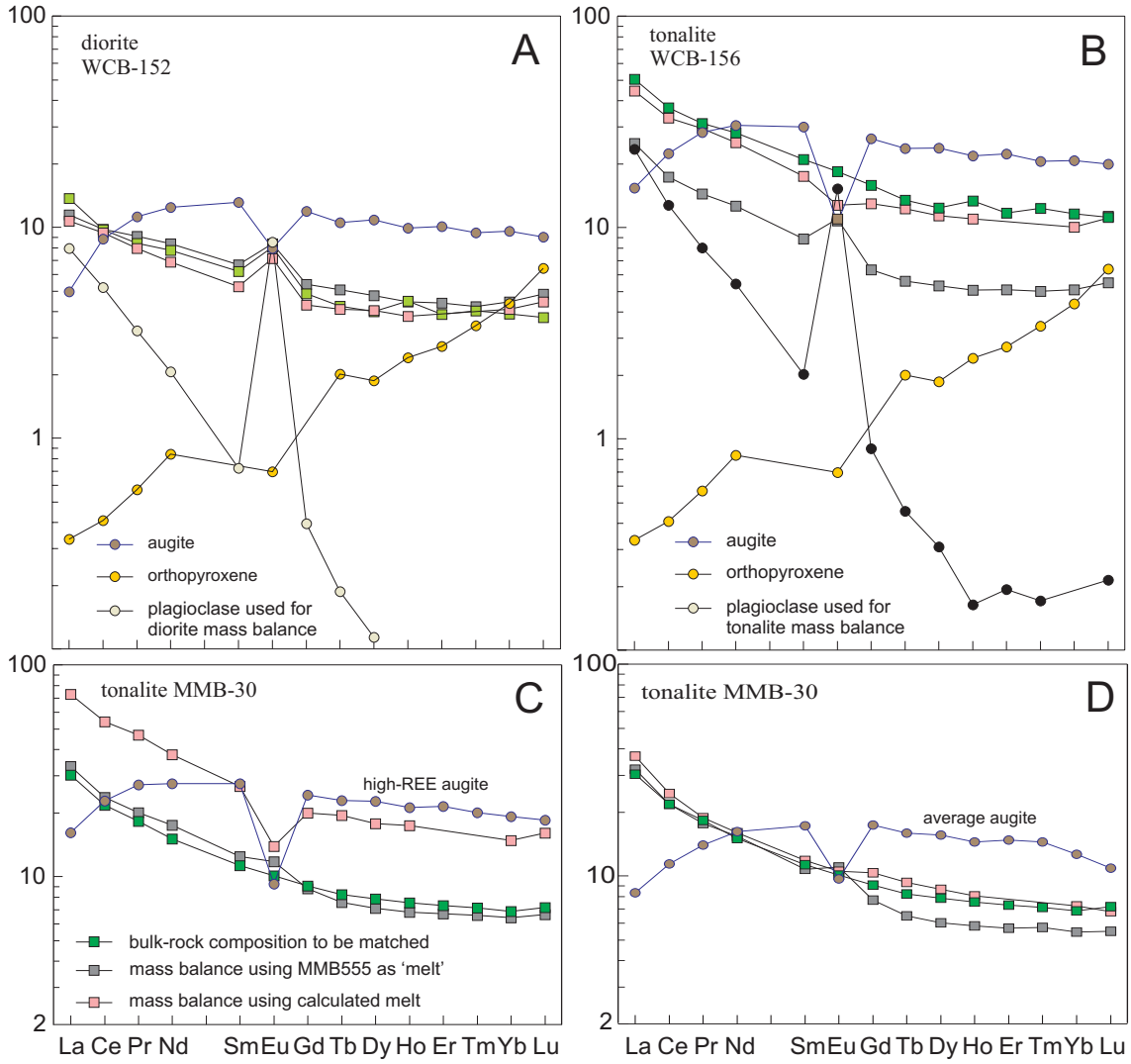
diorite
WCB-152
A
100
10
1
augite
orthopyroxene
plagioclase used for
diorite mass balance
tonalite
WCB-156
B
100
10
1
augite
orthopyroxene
plagioclase used for
tonalite mass balance
tonalite MMB-30
C
high-REE augite
100
10
2
bulk-rock composition to be matched
mass balance using MMB555 as 'melt'
mass balance using calculated melt
La Ce Pr Nd Sm Eu Gd Tb Dy Ho Er Tm Yb Lu
tonalite MMB-30
D
average augite
100
10
2
La Ce Pr Nd Sm Eu Gd Tb Dy Ho Er Tm Yb Lu

Figure 6

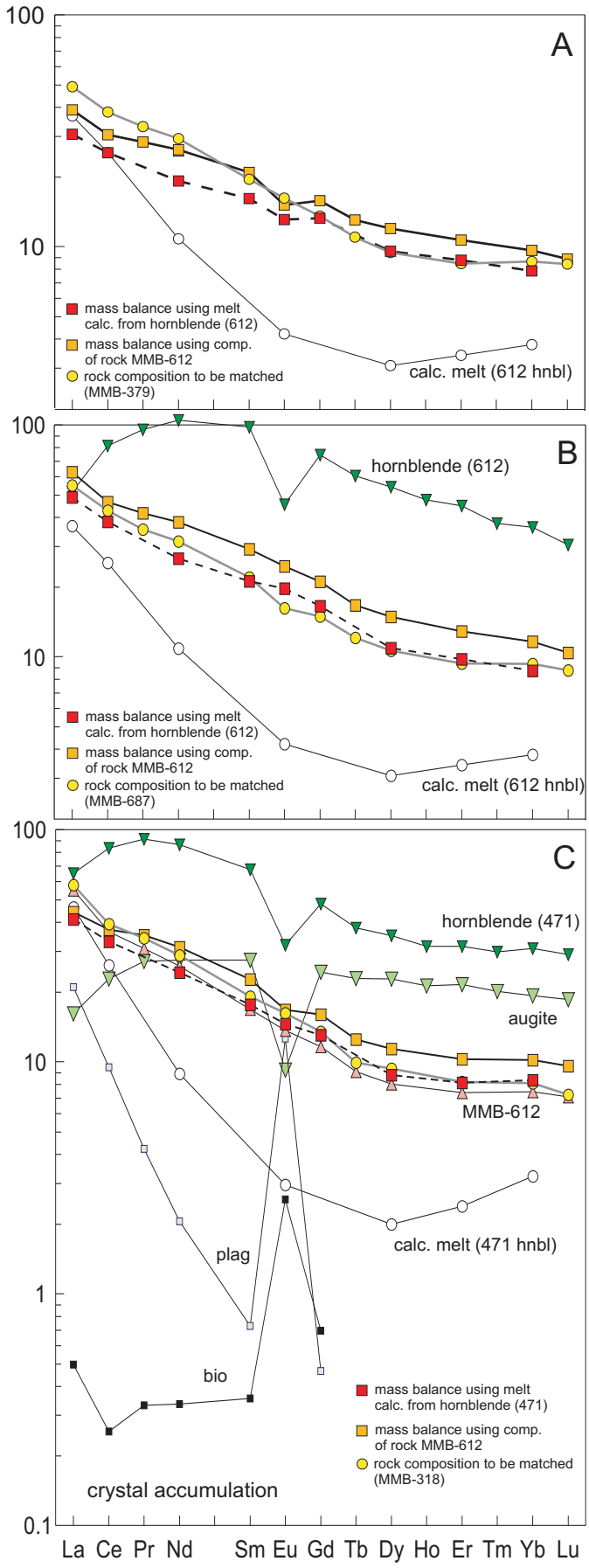
100
10
A
mass balance using melt
calc. from hornblende (612)
mass balance using comp.
of rock MMB-612
rock composition to be matched
(MMB-379)
calc. melt (612 hnbl)
100
10
B
hornblende (612)
mass balance using melt
calc. from hornblende (612)
mass balance using comp.
of rock MMB-612
rock composition to be matched
(MMB-687)
calc. melt (612 hnbl)
100
10
1
0.1
C
hornblende (471)
augite
MMB-612
calc. melt (471 hnbl)
plag
bio
mass balance using melt
calc. from hornblende (471)
mass balance using comp.
of rock MMB-612
rock composition to be matched
(MMB-318)
crystal accumulation
La Ce Pr Nd Sm Eu Gd Tb Dy Ho Er Tm Yb Lu

Figure 7

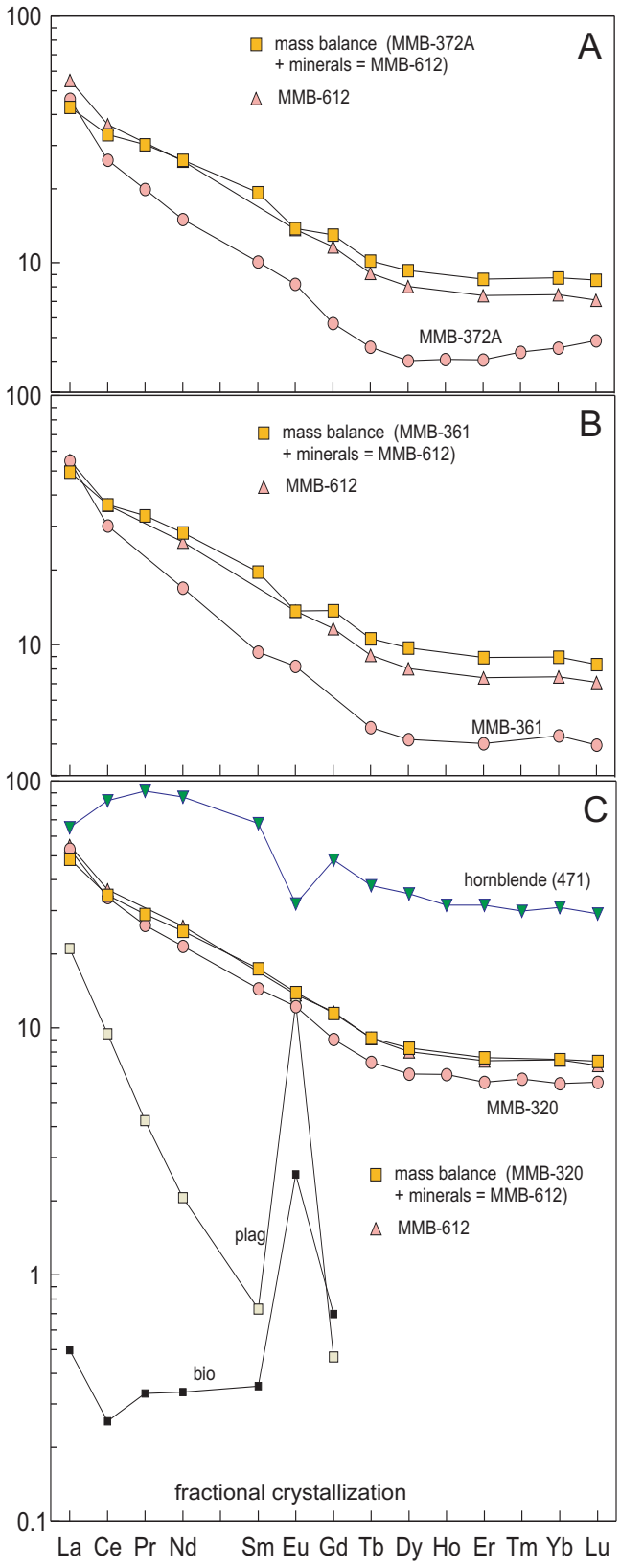
A
mass balance (MMB-372A
+ minerals = MMB-612)
MMB-612
MMB-372A
B
mass balance (MMB-361
+ minerals = MMB-612)
MMB-612
MMB-361
C
hornblende (471)
MMB-320
mass balance (MMB-320
+ minerals = MMB-612)
MMB-612
plag
bio
fractional crystallization
100
10
1
0.1
La Ce Pr Nd Sm Eu Gd Tb Dy Ho Er Tm Yb Lu

Figure 8

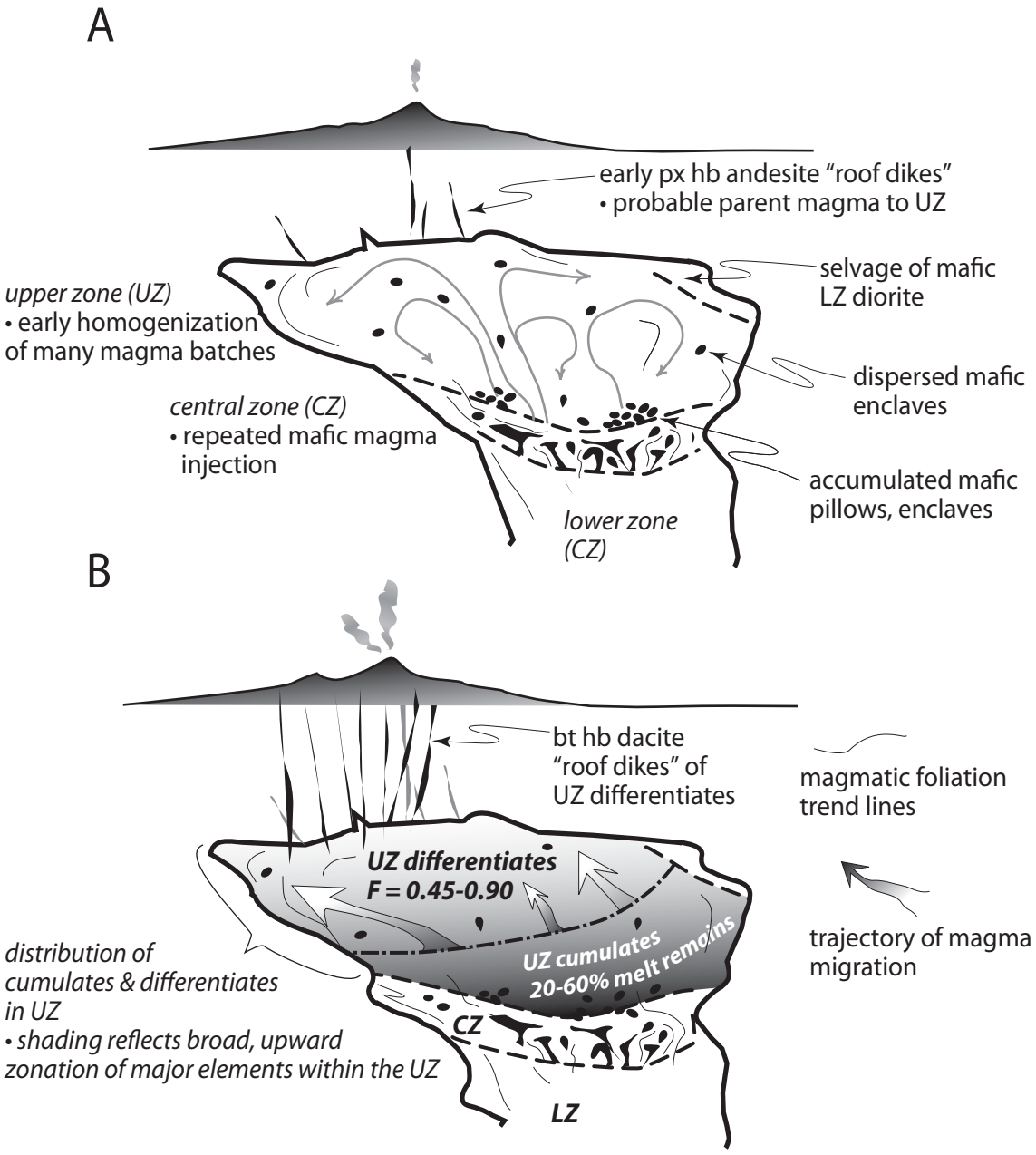
A
early px hb andesite "roof dikes"
• probable parent magma to UZ
selvage of mafic
LZ diorite
upper zone (UZ)
• early homogenization
of many magma batches
dispersed mafic
enclaves
central zone (CZ)
• repeated mafic magma
injection
accumulated mafic
pillows, enclaves
lower zone
(CZ)
B
bt hb dacite
"roof dikes" of
UZ differentiates
magmatic foliation
trend lines
UZ differentiates
F = 0.45-0.90
UZ cumulates
20-60% melt remains
trajectory of magma
migration
distribution of
cumulates & differentiates
in UZ
• shading reflects broad, upward
zonation of major elements within the UZ
CZ
LZ

Figure 9

Table 1. Representative plagioclase and biotite trace element abundances in ppm.

	----------	----------	plagioclase	----------	----------	biotite
sample*	MMB-354	WCB-8	WCB-156	WCB-152	MMB-471	MMB-471
P	70.9	63.3	49.9	69.5	dl	28.8
Zn	5.3	7.0	4.8	3.6	dl	264
Rb	0.95	0.17	0.40	0.26	1.03	375
Sr	489	631	564	556	902	1.76
Y	0.41	0.26	0.18	0.24	0.14	0.52
Zr	1.06	0.14	0.17	0.25	1.27	1.76
Ba	291	260	279	196	280	4776
La	6.96	5.22	6.92	2.46	6.49	0.10
Ce	9.28	8.24	9.24	4.17	7.62	0.08
Pr	0.85	0.69	0.73	0.39	0.51	0.02
Nd	2.58	2.16	2.08	1.24	1.23	0.08
Sm	0.34	0.24	0.20	0.14	0.09	0.01
Eu	0.94	0.88	0.84	0.62	0.92	0.18
Gd	0.20	0.15	0.12	0.10	dl	0.15
Tb	0.021	0.013	0.007	0.009	dl	dl
Pb	12.0	8.3	10.5	2.9	dl	1.36

dl = below detection limits

* samples MMB-354, WCB-8, and WCB-156 are lower zone tonalites

* sample WCB-152 is a lower zone diorite

* sample MMB-471 is an upper zone granodiorite

Table 2. Representative rock compositions used as input to mass balance calculations.

Sample	SiO2	TiO2	Al2O3	Fe2O3	MnO	MgO	CaO	Na2O	K2O	P2O5	LOI	TOTAL	Mg#
Lower zone quartz diorite–tonalite group.													
MMB-15	60.24	0.59	15.28	6.42	0.11	4.22	7.13	2.71	1.38	0.09	2.27	100.44	0.57
MMB-30	60.17	0.53	15.28	6.47	0.13	5.14	7.63	2.45	1.16	0.07	0.37	99.40	0.61
MMB-284	59.00	0.51	15.25	6.69	0.11	5.29	7.72	2.56	1.44	0.07	0.83	99.47	0.61
MMB-293	58.36	0.53	15.44	6.80	0.13	5.29	7.67	2.75	1.37	0.11	0.67	99.12	0.61
MMB-342	56.91	0.48	15.64	7.55	0.14	5.21	8.26	2.65	1.27	0.16	1.23	99.50	0.58
WCB-8	56.34	0.63	16.57	7.67	0.14	5.74	8.39	2.67	1.10	0.13	0.92	100.29	0.60
WCB-156	54.12	0.69	16.89	8.28	0.15	6.03	9.14	2.72	0.78	0.13	0.79	99.72	0.59
Lower zone pyroxenite–diorite group.													
MMB-103	52.92	0.54	16.78	8.41	0.15	6.74	9.35	2.43	1.00	0.19	0.85	99.37	0.61
MMB-121	49.99	0.29	15.54	9.67	0.17	8.97	11.61	1.52	0.28	0.02	2.62	100.68	0.65
MMB-171	50.83	0.61	5.35	12.76	0.25	16.28	12.24	0.58	0.44	0.04	0.71	100.09	0.72
MMB-833A	48.17	0.25	18.38	7.67	0.16	10.62	13.47	0.76	0.12	dl	0.84	100.41	0.73
MMB-833B	51.65	0.39	4.71	8.76	0.19	13.68	18.39	0.58	0.26	dl	0.66	99.27	0.76
WCB-133	50.81	0.50	14.29	9.54	0.19	9.24	11.35	1.91	0.40	0.08	0.48	98.79	0.66
Potential interstitial melts in lower zone mass balance calculations.													
MMB-236A	53.70	0.89	16.41	10.44	0.17	5.53	9.36	2.77	1.43	0.19	dl	100.88	0.51
MMB-555	51.99	0.89	15.90	10.23	0.18	5.74	9.41	2.73	1.41	0.21	0.74	99.43	0.53
MMB-771	49.92	1.01	17.55	10.27	0.19	6.02	9.92	2.64	0.72	0.27	0.93	99.44	0.54
MMB-777A	65.57	0.46	15.87	4.49	0.08	2.19	4.77	3.29	2.41	0.13	0.81	100.08	0.49
WCB-4809	53.01	0.88	18.35	8.55	0.14	5.23	8.94	3.05	1.15	0.26	0.91	100.46	0.55
Upper zone samples.													
MMB-208	57.87	0.65	17.19	7.05	0.12	3.48	6.98	3.32	1.78	0.18	1.14	99.76	0.49
MMB-318	53.81	0.75	17.32	8.34	0.14	4.25	8.14	3.12	1.77	0.20	1.48	99.32	0.50
MMB-320	65.51	0.45	15.07	4.59	0.10	2.57	4.44	3.31	2.64	0.16	1.07	99.90	0.53
MMB-361	70.10	0.21	15.50	2.68	0.06	1.11	2.97	3.58	3.41	0.07	0.80	100.49	0.45
MMB-372A	70.65	0.27	14.37	2.55	0.06	1.16	2.90	3.71	3.34	0.08	0.48	99.57	0.47
MMB-379	55.95	0.59	16.18	7.83	0.15	5.24	7.83	3.04	1.44	0.18	1.31	99.74	0.57
Composition used as parental magma for upper zone mass balance calculations.													
MMB-612	60.67	0.53	16.02	6.36	0.11	3.14	6.00	3.33	2.36	0.16	1.41	100.09	0.49

dl = below detection limits

Data from Barnes (1983), Barnes et al. (1986a, 1990), Coint et al. (2013b)

Mg# = Mg/(Mg+Fe)

Table 3. Lower zone major element mass balance results.

Sample	rock type	'melt'	% 'melt'	% augite	% opx	% plag	%Fe-Ti oxide	r²	plag/(plag+px+oli	Notes
pyroxenite to diorite group										
MMB833A	diorite	MMB771	7.2	21.9	0.0	51.9	0.0	0.87	0.56	An77; 18.7% Fo72
MMB833B	melagabbro	MMB236A	14.5	72.3	4.2	4.5	0.0	0.02	0.05	An73; 2.0% Fo72
MMB833B	melagabbro	MMB771	18.4	71.7	6.2	1.8	0.0	0.02	0.02	An85
MMB171	pyroxenite	WCB4809	7.5	43.6	37.4	7.7	0.0	0.95	0.09	An73
MMB171	pyroxenite	WCB4809	5.0	44.9	36.6	9.5	1.1	0.30	0.10	An73
MMB171	pyroxenite	MMB771	14.1	41.6	35.6	5.4	0.0	0.50	0.07	An85
MMB121	gabbro	MMB236A	25.1	17.1	19.9	33.9	1.0	0.02	0.48	An77
MMB121	gabbro	MMB771	50.9	14.5	15.1	18.3	0.0	0.14	0.38	An85
WCB128A	diorite	WCB4809	34.5	9.8	25.7	6.4	0.4	1.02	0.15	An73; *
WCB133	quartz diorite	MMB555	66.8	15.3	10.3	7.5	0.0	0.04	0.23	An78
MMB103	quartz diorite	WCB4809	83.0	6.3	5.7	4.6	0.0	0.32	0.28	An73
MMB103	quartz diorite	MMB555	50.0	7.3	13.1	29.0	0.0	0.50	0.59	An50
WCB152	diorite	WCB4809	31.8	14.5	20.0	33.6	0.7	0.07	0.49	An77
WCB152	diorite	MMB555	19.3	19.2	21.3	41.6	0.0	0.20	0.51	An73
MMB351	quartz diorite	MMB555	48.4	9.0	14.7	27.4	0.6	0.09	0.54	An60; *
quartz diorite to tonalite group										
WCB6809	quartz diorite	MMB548	27.7	9.0	21.5	39.8	2.0	0.31	0.57	An60; *
WCB808	(quartz) diorite	MMB548	41.3	9.7	16.4	32.1	1.1	0.08	0.55	An60; *
MMB354	tonalite	MMB548	70.3	11.7	6.4	12.4	0.0	0.62	0.41	An60
MMB354	tonalite	MMB777A	58.0	13.8	0.9	19.1	0.0	0.39	0.57	An50
WCB156	tonalite	MMB548	33.8	9.3	18.9	36.2	0.0	0.30	0.56	An68; *
WCB156	tonalite	MMB777A	31.4	11.3	18.0	36.8	1.0	0.10	0.56	An68
MMB594	quartz diorite	MMB548	48.5	10.4	14.0	26.2	1.7	0.07	0.52	An73
MMB594	quartz diorite	MMB777A	40.9	7.4	19.3	31.0	1.3	0.38	0.54	An68
MMB293	tonalite	MMB548	58.2	10.2	11.4	19.9	0.3	0.08	0.48	An60
MMB293	tonalite	MMB777A	52.1	10.5	13.6	22.5	0.0	0.08	0.48	An60
MMB430A	tonalite	MMB548	54.6	7.9	11.8	25.3	0.2	0.27	0.56	An60
MMB342	tonalite	MMB548	52.0	12.2	10.5	23.6	1.5	0.10	0.51	An60; *
MMB111	tonalite	MMB777A	38.4	11.7	16.1	33.4	0.3	0.29	0.55	An50
MMB30	tonalite	MMB777A	55.5	14.5	8.5	21.2	0.0	0.42	0.48	An50
MMB15	tonalite	MMB777A	63.0	11.9	5.8	17.4	0.7	0.15	0.50	An50
MMB284	tonalite	MMB777A	54.9	11.7	12.3	20.3	0.0	0.10	0.46	An60

* includes trace apatite

r^2, sum of squares of residual errors

Abbreviations: plag, plagioclase; px, pyroxene; opx, orthopyroxene; oliv, olivine; Fo, mole fraction forsterite in olivine; An, mole fraction anorthite in plagioclase

'melt' = rock composition used to model interstitial melt

Table 4. Upper zone major element mass balance results.

Fractional crystallization from composition MMB-612

daughter	rock type	SiO_2	% daughter	% hnbl	% biotite	% plag	% px	%Fe-Ti oxide	%apatite	r^2	plag/ (plag+mafic)	plag comp	% residual melt
MMB-471	granodiorite	62.05	91.8	4.6	0.0	2.8	0.0	0.5	0.0	0.02	0.38	An43	92
MMB-320	granodiorite	65.51	73.5	10.0	1.7	13.8	0.0	0.6	0.0	0.05	0.54	An56	73
MMB361	granodiorite	70.1	58.9	20.7	1.6	17.6	0.0	0.4	0.0	0.03	0.44	An56	59
MMB372A	granite	70.65	53.6	20.4	2.8	22.4	0.0	0.4	0.0	0.06	0.49	An50	54
average											0.46		

Accumulation from melt of composition MMB-612

daughter	rock type	SiO_2	% 'melt'	% hnbl	% biotite	% plag	% px	%Fe-Ti oxide	%apatite	r^2	plag/ (plag+mafic)	plag comp	% insterst melt
MMB331	qtz diorite	53.12	36.9	22.7	7.2	26.2	5.9	0.0	0.0	0.06	0.42	An50	37
MMB318	qtz monzodiorite	53.81	43.0	22.6	4.6	28.4	0.0	0.2	0.6	0.08	0.51	An50	43
MMB379	tonalite	55.95	48.6	8.4	0.0	26.1	15.5	0.2	0.2	0.05	0.52	An50	49
WCB7709	tonalite	56.31	55.0	15.1	4.3	25.8	0.0	0.0	0.5	0.01	0.57	An50	55
MMB208	qtz monzodiorite	57.87	70.9	11.6	0.0	17.0	0.0	0.4	trace	0.06	0.59	An50	71
MMB208	qtz monzodiorite	57.87	70.9	10.9	1.4	16.8	0.0	0.0	0.0	0.06	0.58	An50	71
MMB397	tonalite	58.02	73.4	2.6	4.3	11.3	9.0	0.0	0.0	0.11	0.42	An56	73
MMB687	diorite	58.34	79.7	14.4	0.0	5.2	1.2	0.0	0.1	0.05	0.25	An56	80
MMB687	diorite	58.34	79.4	15.7	0.0	5.3	0.0	0.0	0.3	0.07	0.25	An50	79
Z1	tonalite	58.59	75.3	11.7	0.0	13.4	0.0	0.1	0.1	0.05	0.53	An50	75
MMB317	qtz monzodiorite	58.71	77.6	8.8	0.0	12.8	1.3	0.0	0.1	0.09	0.56	An56	78
MMB317	qtz monzodiorite	58.71	76.3	10.9	0.0	13.3	0.0	0.2	0.2	0.08	0.55	An50	76
average											0.48		

r^2, sum of squares of residual errors
plag, plagioclase; px, pyroxene; hnbl, hornblende; An, mole fraction anorthite in plagioclase
'melt' = rock composition used to model interstitial melt